

178  
94

CHARACTERIZATION OF HIGH TEMPERATURE CREEP IN SILICONIZED SILICON  
CARBIDE USING ULTRASONIC TECHNIQUES

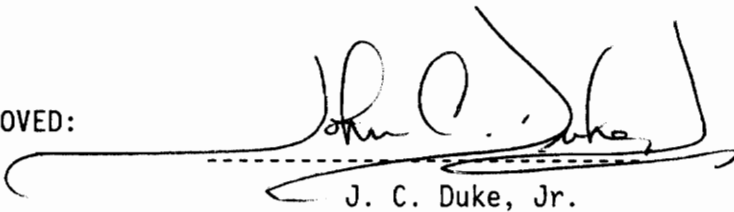
by

Jonathan D. Buttram

Thesis submitted to the Faculty of the  
Virginia Polytechnic Institute and State University  
in partial fulfillment of the requirements for the degree of

Master of Science  
in  
Engineering Science and Mechanics

APPROVED:



J. C. Duke, Jr.



W. W. Stinchcomb



M. S. Cramer

April 1990  
Blacksburg, Virginia

LD

5655

V855

1990

B988

C.2



CHARACTERIZATION OF HIGH TEMPERATURE CREEP IN SILICONIZED SILICON  
CARBIDE USING ULTRASONIC TECHNIQUES

by

Jonathan D. Buttram

Committee Chairman: J. C. Duke, Jr.  
Engineering Mechanics

(ABSTRACT)

Ultrasonic velocity and attenuation were both measured on samples containing various degrees of damage due to high temperature creep. These results were compared with parameters associated with creep damage such as strain and cavity formation, in order to better understand the mechanisms of creep in Si/SiC and to determine if ultrasonics can be used in evaluating the severity of damage.

The data indicated that both ultrasonic velocity and attenuation are directly related to creep strain and can be used in evaluating creep damage. Ultrasonic velocity was found to be exponentially related to creep strain. Cavity formation was found not to significantly affect either of the measured ultrasonic properties.

The results indicated that Si/SiC behaves as a two phase material in that high frequency ultrasound propagates primarily through the silicon carbide phase and not by the silicon phase.

## TABLE OF CONTENTS

| Chapter  | Page |
|--|------|
| I. INTRODUCTION.....                             | 1    |
| II. HIGH TEMPERATURE CREEP OF CERAMICS.....      | 4    |
| Sintered Silicon Carbide.....                    | 5    |
| Siliconized Silicon Carbide.....                 | 10   |
| III. ULTRASONIC THEORY AND RELATED RESEARCH..... | 13   |
| Ultrasonic Attenuation.....                      | 13   |
| Ultrasonic Velocity.....                         | 18   |
| IV. EXPERIMENTAL METHODS.....                    | 21   |
| Samples.....                                     | 21   |
| Sound Attenuation Measurements.....              | 26   |
| Sound Velocity Measurements.....                 | 35   |
| V. RESULTS.....                                  | 40   |
| Microstructural Analysis.....                    | 40   |
| Sound Attenuation Measurements.....              | 50   |
| Sound Velocity Measurements.....                 | 57   |
| VI. ERROR ANALYSIS.....                          | 68   |
| Ultrasonic Attenuation Measurements.....         | 68   |
| Velocity Measurements.....                       | 69   |
| VII. CONCLUSIONS.....                            | 73   |
| REFERENCES.....                                  | 75   |
| VITA.....  | 77   |

## LIST OF FIGURES

| Figure  | Page |
|---|------|
| Figure 1: Diffusional Creep.....  | 7    |
| Figure 2: Formation of Cracks Due to Grain Boundary Sliding.....                                    | 9    |
| Figure 3: Creep Process in Siliconized Carbide.....   | 12   |
| Figure 4: The Basic Loss Mechanisms Involved In The Scattering<br>of Ultrasound.....                | 15   |
| Figure 5: Gage Section From A Typical Si/SiC Creep Sample.....                                      | 24   |
| Figure 6: Exponentially Decaying Echo Train Necessary For<br>Accurate Attenuation Measurements..... | 27   |
| Figure 7: Schematic of Equipment Used For Ultrasonic Attenuation<br>Measurements.....               | 30   |
| Figure 8: Transducer/Aperture Used In Attenuation Measurements.....                                 | 32   |
| Figure 9: Pulse-Echo Overlap Technique.....   | 36   |
| Figure 10: Equipment Used For Velocity Measurements.....  | 38   |
| Figure 11: Microstructure of "As Received" Siliconized<br>Silicon Carbide (200X).....               | 41   |
| Figure 12: Micrographs of Samples Tested at 1300°C (200X).....                                      | 42   |
| Figure 12: (Continued).....   | 43   |
| Figure 13: Micrographs of Samples Tested at 1375°C (200X).....                                      | 44   |
| Figure 13: (Continued).....   | 45   |
| Figure 14: Cavity Density Verses Percent Creep Strain Plot<br>For All Samples Tested.....           | 48   |

|   |    |
|---|----|
| Figure 15: Volume Fraction Cavities Verses Percent Creep Strain<br>For All Samples Tested.....                                    | 49 |
| Figure 16: Material Sound Attenuation Verses Percent Creep Strain...  | 52 |
| Figure 17: Material Sound Attenuation Verses Cavity Density.....  | 54 |
| Figure 18: Material Sound Velocity Verses Percent Creep Strain.....   | 59 |
| Figure 19: Material Sound Velocity Verses Volume Fraction Cavities..  | 60 |
| Figure 20: Plot of Material Sound Velocity Versus Percent Creep<br>Strain Showing Curve of Theoretical Model .....                | 65 |
| Figure 21: Material Sound Velocity Verses Material Density.....   | 67 |
| Figure 22: Plot Illustrating The Scatter In Attenuation Data<br>Associated With Measurements Taken At Different<br>Locations..... | 70 |
| Figure 23: Plot Illustrating The Scatter In Velocity Data<br>Associated With Measurements Taken At Different<br>Locations.....    | 72 |

## LIST OF TABLES

| Table   | Page |
|---|------|
| Table 1 Siliconized Silicon Carbide Creep Test Data.....  | 23   |
| Table 2 Thickness of Each Sample Measured At The Area<br>To Be Tested Ultrasonically.....         | 25   |
| Table 3 Cavity Density Volume Fraction And Material Density<br>Data for Si/SiC Creep Samples..... | 47   |
| Table 4 Average Ultrasonic Attenuation Data Taken On Each Sample...                               | 51   |
| Table 5 Average Ultrasonic Velocity Data Taken On Each Sample.....                                | 58   |

## ACKNOWLEDGMENTS

I would like to express thanks to Dr. John C. Duke for his assistance and guidance throughout most of my college career as well as with this thesis.

Also a special thanks to Dr. S. M. Wiederhorn and Dan Carroll at National Institute of Standards and Technology for letting me use their samples and creep data and Dr. Don Stevens and the entire crew in NDM&D at the Lynchburg Research Center for letting me use their equipment. This thesis would not have been possible without the cooperation of these individuals.

I would also like to express my thanks to Jeff Barefoot and Walter Koch for their support as both friends and roommates, my grandmother Mrs J. P. Roudabush for just being a perfect grandmother and Lisa Rigney for putting up with me these last few months.

Finally, I would like to dedicate this thesis to my parents, Mr. and Mrs. Jimmy W. Buttram, Sr. who supported me emotionally and financially throughout this endeavor. Thanks again.

## Chapter I

### INTRODUCTION

Structural ceramics are envisioned as playing an important role as a major engineering material in the future. New engineering applications are requiring the use of materials that can perform in ever increasing temperature ranges. Research over the last decade on high performance materials has focused on those materials that can replace metals in high temperature engineering applications. The decreasing supply of metals such as Cr, Co, Ni and Ti and the increasing emphasis on energy conservation accompanied with the desire to use that energy more efficiently has made high temperature structural ceramics leading contenders as engineering materials.

Desirable properties such as high temperature strength, chemical stability, low thermal expansion, resistance to oxidation, irradiation and thermal shock, and a high modulus of elasticity make ceramics unique candidates for many applications. Presently ceramics can be found in uses such as bearings, piston rings, combustion chambers, nozzles, heat exchangers, heating elements, chemical plant components, etc.<sup>(1)</sup> Some proposed uses include high performance turbine components, engine hot section components and containment material for



nuclear purposes.(2) However ceramic materials have two basic disadvantages, a low fracture toughness and a wide variation in strength properties, that presently prohibit their use in more structurally critical areas. It is interesting to note that the variable strength and fracture toughness can be generally attributed to discrete defects such as inclusions, voids and cracks that are an undesirable result of the manufacturing process. Current cost-effective fabrication procedures also frequently produce ceramics containing bulk density variations and microstructural abnormalities that can adversely affect performance. Therefore it is imperative that processing techniques be improved and/or nondestructive evaluation methods by which to inspect the product subsequent to processing be developed. These nondestructive evaluation methods (NDE) would not only have to be able to detect discrete flaws but must also characterize microstructural and morphological factors which ultimately govern the strength, toughness and dynamic performance of the ceramic. It has been suggested that NDE methods would not only improve the confidence in the quality of a ceramic but also could provide valuable information that could be used in improving

fabrication procedures.(3) Therefore it is evident that NDE is critical to the successful use of structural ceramics in the future. It was with these considerations in mind that the objective of this Master of Science Thesis was formulated.

The purpose of this Master of Science Thesis was to study the effects that high temperature creep of siliconized silicon carbide (SiC) has on ultrasonic attenuation and velocity. This investigation also explores the contributions that variations in density and microstructure have on the ultrasonic measurements. The ultimate goal is to find a nondestructive method that will effectively characterize the amount of high temperature creep damage that has occurred and to determine what changes are occurring in the material that affect these ultrasonic measurements.

## Chapter II

## HIGH TEMPERATURE CREEP OF CERAMICS

High temperature properties such as thermal expansion, thermal conductivity and thermal shock all help determine the temperature resistance of a ceramic material. Another high temperature property that must be considered is a ceramic material's resistance to high temperature creep. Although this property is not generally associated with ceramic materials, given the proper temperatures and loads, a ceramic material can fail as a result of creep. If not controlled, high creep rates can lead to excessive deformation and uncontrolled stress.

Creep is a thermally activated process that can generally be described by three different stages. The first or primary stage, begins immediately after loading usually in temperatures above approximately 1000°C for ceramic materials. During the primary stage, the creep rate decreases continuously until a steady state or secondary creep stage is reached. During the secondary stage the creep rate is effectively constant. It is also in this stage that most structural ceramics would operate for a significant time before failure. Therefore the secondary creep rate is considered the most

important creep related property of ceramics for structural applications. Finally the formation of cracks, cavities, etc., becomes extensive enough to affect the creep rate. This increase in the creep rate indicates the beginning of the final creep stage, the tertiary stage. It is in this stage that the ceramic material will fail.(4)

Various mechanisms can be responsible for the plastic deformation experienced during the different stages of creep of an engineering ceramic. In fact, these mechanisms can differ greatly depending upon the ceramic being considered. The following paragraphs will address the creep mechanisms associated with both sintered silicon carbide and siliconized silicon carbide in an attempt to clarify the differences in these two materials.

#### Sintered Silicon Carbide

Simon and Bunsell(5) suggest that the decreasing creep rate experienced during the primary creep stage is mainly due to a recrystallization process. Their work using SiC fibers suggest that the recrystallization process involves a rapid increase of crystal size with initial loading at temperature above 1000°C. After a finite time the crystalline structure stabilizes and a creep process

involving defect migration may then predominate. Mechanisms that contribute to the creep process during the secondary creep stage are slip, dislocation climb, diffusional creep, grain boundary movement and twinning.<sup>(6)</sup> The predominating mechanism varies depending upon the ceramic material being studied. Krishnamachari and Notis conclude that grain boundary diffusion is the most likely creep controlling process in silicon carbide.<sup>(2)</sup> Although they do not discount other mechanisms as contributing to creep, they do state that dislocation movement would be difficult in SiC because of the covalent bonding, the limited number of slip systems available in the hexagonal structure, and the high melting point. Grain boundary diffusion is a process where vacancies diffuse along the grain boundaries of a material (Coble creep) as opposed to vacancies diffusing from one end of a grain to its sides through the grain (Nabarro-Herring creep) as shown in Figure 1. It should be noted that although grain boundary diffusion is considered the creep controlling mechanism for SiC, it is not solely responsible for all creep. Grain boundary sliding is also a contributing mechanism because grain boundary movement always accompanies diffusional creep.<sup>(6)</sup> Also sintered SiC can experience grain boundary sliding caused by the presence of a continuous Si phase

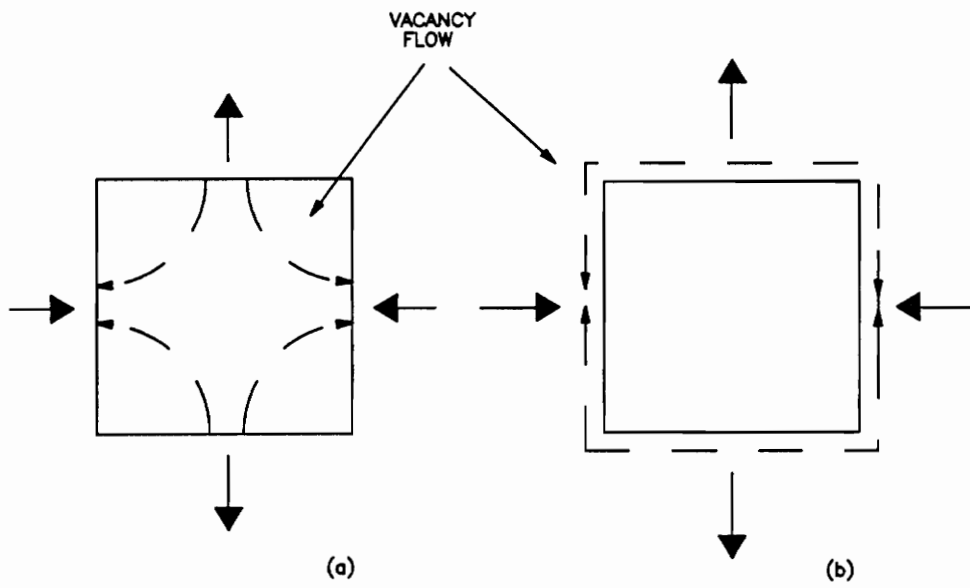


Figure 1:

Diffusional Creep: a) Nabarro-Herring  
b) Coble Creep  
(Grain Boundary Diffusion)

which is near its melting point under test conditions. The presence of this glassy phase at the grain boundaries can lessen the forces required for relative grain movement.<sup>(7)</sup> It is grain boundary movement that directly affects the start of the tertiary stage by initiating grain boundary cracking. Grain boundary cracking is a result of a buildup of tensile stresses at grain boundaries induced by relative movement of neighboring grains. If these stresses are not relieved by further plastic deformation then cracking and the formation of cavities can occur causing inter-granular failure as shown in Figure 2. This type of failure should directly affect the bulk density of the damaged material. Other microstructural defects can also have an effect on the creep rate of a ceramic. Porosity for example, has been shown to increase creep rates by effectively increasing deformation at grain boundaries along with having a stress concentrating effect. The presence of impurities, especially at grain boundaries, can actually help control creep rates by restricting the grain boundary diffusion processes. However these same impurities can also promote grain boundary sliding by forming a glassy phase at the boundaries.

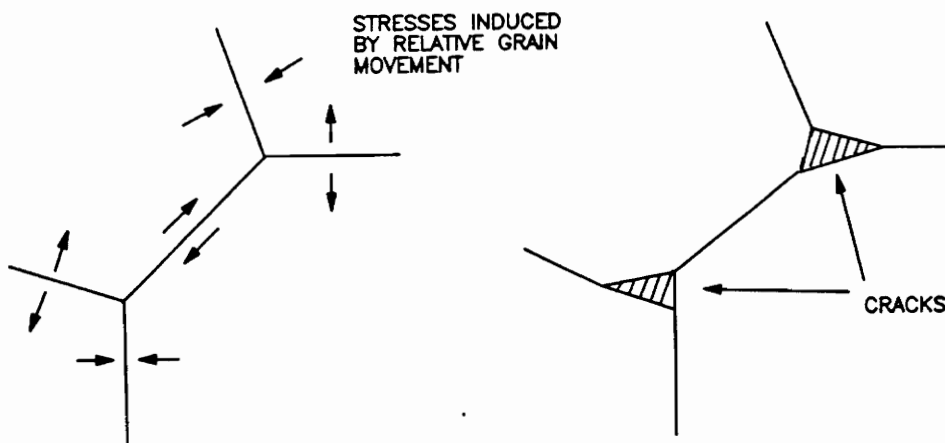


Figure 2:  
Formation of Cracks Due to Grain Boundary Sliding.



### Siliconized Silicon Carbide:

Siliconized silicon carbide is considered a composite material due to its internal structure where a silicon carbide network is surrounded by a matrix of pure silicon. This microstructure is produced when a silicon carbide compact is infiltrated with pure silicon at high temperatures ( $1600^{\circ}\text{C}$ ) during the manufacturing process. This process yields a nearly 100% dense material consisting of two independently interconnected crystalline phases.

High temperature creep studies performed by S.M. Wiederhorn(8-11) on siliconized silicon carbide have produced creep curves exhibiting primary, steady state and tertiary creep modes. These modes are a result of a deformation process much different than that occurring in a sintered silicon carbide ceramic. Wiederhorn suggests that two mechanisms, silicon deformation and cavity formation, control the creep process. At high temperatures (above  $1100^{\circ}\text{C}$ ), the silicon matrix becomes highly ductile when compared to the rigid silicon carbide particles. Initial stress, prior to any deformation, is supported primarily by the network composed of bonded silicon carbide grains. As the stress increases, failure and slippage occurs at the SiC grain

contact points causing some dislocation structures to form within the grains. (See Figure 3) This relative movement between grains or grain clusters initializes the creep process primarily by redistributing the stress to the more plastic silicon matrix. This in turn causes the silicon to flow around the SiC grains in an effort to relieve hydrostatic stresses caused by this movement. If the silicon flow is not adequate, negative pressure can develop in the areas of the Si/SiC interfaces, giving rise to the formation of cavities. Wiederhorn found that cavities are more likely to form at Si/SiC interfaces that are normal to the stress field. It was determined that the formation of cavities affect the slope of the creep curve. As deformation of the ceramic increases the cavities will tend to align and will eventually cause the formation of cracks. These cracks directly lead to the failure of the ceramic and mark the beginning of the tertiary stage of creep.

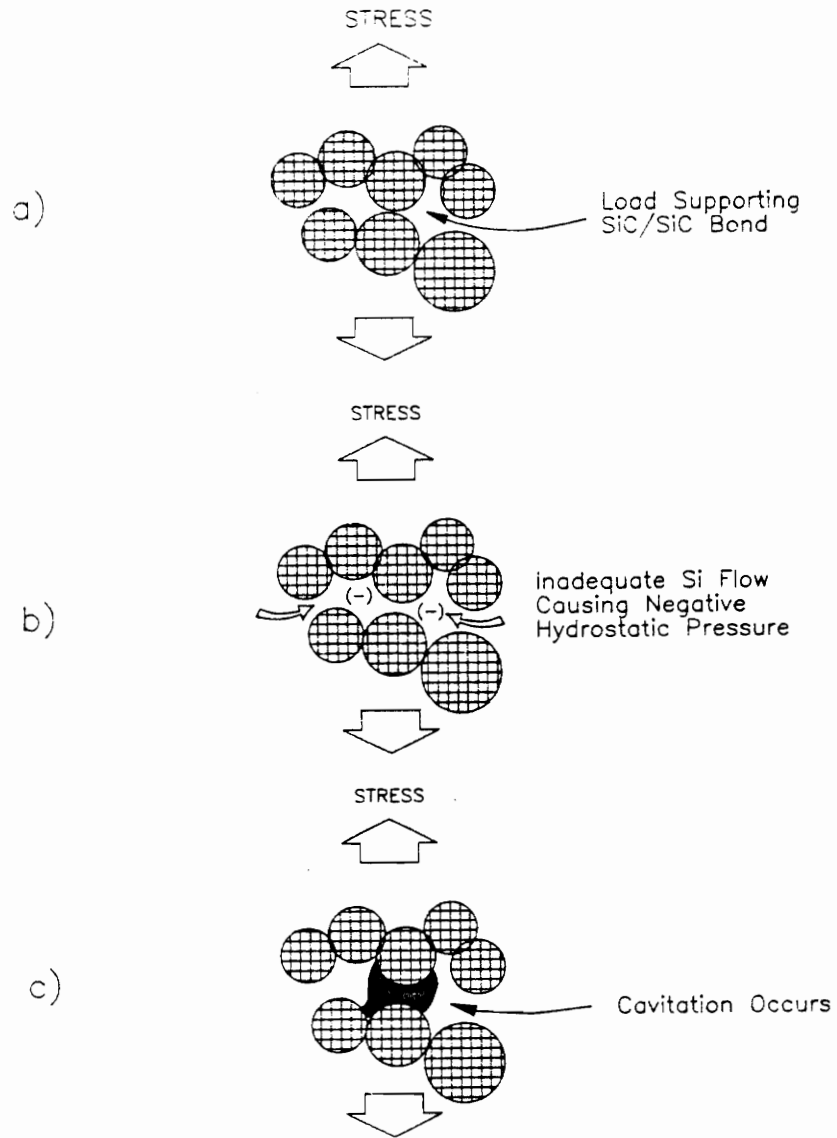


Figure 3:

Creep Process in Siliconized Silicon Carbide: a) SiC Intergranular Failure b) Relative Grain Movement and Silicon Flow c) Cavity Formation

## Chapter III

## ULTRASONIC THEORY AND RELATED RESEARCH

## ULTRASONIC ATTENUATION

Ultrasonic attenuation is the gradual loss of ultrasonic energy as it travels through a material. Two major sources of ultrasonic attenuation exist for polycrystalline materials in the megahertz range. These are hysteresis and scattering losses. Hysteresis losses are caused by the anelastic behavior of a material as a stress wave propagates through it. The total contribution of hysteresis losses is not considered significant unless the frequency of the attenuated signal falls at either end of the megahertz frequency spectrum (12). Therefore only "scattering" losses will be considered due to the frequencies used for attenuation testing in this investigation (center frequency approximately 70 MHz).

There are three distinct types of scattering phenomenon that can occur as a result of an interaction between ultrasound and a material's microstructure. These are namely Rayleigh, phase and diffusion scattering. The predominating scattering mechanism depends directly on the ratio of the wavelength ( $\lambda$ ) to the average grain

diameter ( $\bar{D}$ ). Figure 4 summarizes the three loss mechanisms along with the attenuation associated with each. Here  $f$  is the frequency and  $\Delta K/K$  is the direction related average change in elastic properties of the grains encountered by the ultrasound. It should be noted that these equations are very general and do not account for hysteresis losses, thermoelastic losses, and mode conversion losses that have been included among other theories.<sup>(12)</sup>

As indicated by Figure 4, Rayleigh scattering occurs when  $\lambda \gg \bar{D}$ , (i.e., the wavelength is much larger than the average grain diameter). Here, the entire grain acts as the scattering unit. When  $\lambda \ll \bar{D}$ , diffusion scattering predominates. Diffusion scattering is associated with mean free path considerations. Here individual grain boundaries affect the scattering process. Because the number of grain boundaries encountered directly affects the amount of scatter, diffusion scattering is inversely dependent upon grain size. Finally, phase scattering is a process that occurs when the wavelength is approximately equal to the average grain diameter. This mechanism is a result of the random orientation of various grains. These variations in orientation causes each grain to appear to have different elastic properties thus propagating the ultrasound at

| WAVELENGTH TO<br>GRAIN DIAMETER<br>RANGE | MECHANISM | ATTENUATION                                 |
|--|-----------|---|
| $\lambda \gg \bar{D}$                    | RAYEIGH   | $\overline{\{\Delta K/K\}^2} \bar{D}^3 f^4$ |
| $\lambda \approx \bar{D}$                | PHASE     | $\overline{\{\Delta K/K\}^2} \bar{D} f^2$   |
| $\lambda \ll \bar{D}$                    | DIFFUSION | $\overline{\{\Delta K/K\}^2} \bar{D}^{-1}$  |

Figure 4:

Three Basic Loss Mechanisms Involved In The Scattering  
of Ultrasound(12)

different velocities through each grain. As a result of this, the received signal will contain numerous phase variations. The summation of such phase variations within the ultrasonic signal could result in a loss of energy. The amount of attenuation is also influenced by factors such as the grain size, grain size distribution, crystallographic anisotropy of the grain, grain orientation, nonequiaxed grains, or polyphased grain structures.

In addition to grain structure, ultrasonic attenuation is also dependent upon other microstructural abnormalities such as porosity, inclusions, etc.. In general, an inhomogeneity will scatter elastic waves if it differs in elastic properties or density from the surrounding medium<sup>(13)</sup>. Therefore it is clear that porosity for instance, can attenuate in much the same manner that grains do. In fact it is possible that these type of abnormalities can impede the transmission of ultrasound more efficiently than the grain structure.

Results of related research have shown that various factors can influence the attenuation of ultrasound in silicon carbide. Klima (14) compared the attenuation of small and large grained samples that had similar density values. He concluded that grain size did have a significant affect on attenuation. He also observed that the less

attenuating material had equiaxed grains while many grains in the more attenuating material were elongated or rodlike in shape. He also noted that the larger grained material contained larger pores that were distributed less densely which could have affected the attenuation measurements. In contrast, Baaklini, Generazio and Kiser (15) found that attenuation was not due to grain boundary scattering in sintered silicon carbide. They concluded that pore site scattering was the main attenuation mechanism. They found that pore site scattering was dependent upon the average pore size and the porosity distribution. They reported that for an average increase in pore size of 115 % the mean attenuation coefficient increased by 300 %. They also found a strong relationship between attenuation and density. For a 1.97 % increase in density, they found that the attenuation decreased 150 %.

It should be noted that a thorough literature search covering the topics discussed in this report produced no previous research that directly linked high temperature creep damage to ultrasonic sound attenuation measurements.



### Ultrasonic Velocity

The velocity of longitudinal sound waves as they pass through a homogeneous solid is related to that material's elastic constants by the following expression:

$$V_l^2 = \frac{E}{\rho} \frac{(1-\mu)}{(1+\mu) + (1-2\mu)} \quad (1)$$

where  $E$  is the elastic modulus,  $\rho$  is the density, and  $\mu$  is Poisson's ratio. It should be noted that equation 1 may not apply to Si/SiC due to its two phased structure. As previously discussed, an expected result of high temperature creep strain is a gradual decrease in density due to the formation of micro-voids in the ceramic microstructure. The effect of a decrease in density on longitudinal wave velocity may not be what is obviously implied by Equation 1. Klima and Watson<sup>(16,17)</sup> predict that a decrease in density should produce a decrease in longitudinal velocity. They say that this result is due simply to the fact that sound velocity is higher in a solid than in a gaseous medium. Because the sound will have to pass through more of this gaseous medium as the porosity increases, the resulting average sound velocity will drop. Further work by Klima and Baaklini attempt to explain this relationship in a more detailed

manner. They pointed out studies that have shown Young's modulus to increase exponentially with increasing density (ie. as porosity decreases):

$$E = E_0 \exp (-bP) \quad (2)$$

where  $E_0$  is Young's modulus for the nonporous material,  $P$  is the volume fraction porosity and  $b$  is a porosity correction factor determined by pore shape, size, location, etc. They also state that Poisson's ratio generally increases with increasing density, but this effect is relatively small. Therefore they concluded that the exponential change in Young's modulus is the controlling factor in density related changes in the longitudinal velocity<sup>(3)</sup>. Studies using SiC have shown that longitudinal velocity increases with an increase in density<sup>(3,14,15,16,18)</sup>. In most cases, a 1 percent change in density of a sample produced a 1 percent change in the velocity measurement. However, there are some minor discrepancies concerning the effect that microstructural variations have on sound velocity measurements. Although sound velocity should not be affected by grain

size, results of various investigations using SiC indicate differently. Generally it has been found that the velocity for larger grained materials is slightly higher than that of the smaller grained samples(3,14,16). This observation implies that larger grained materials have a higher modulus of elasticity. This, however, cannot be a direct result of the larger grains themselves due to the fact that elastic properties (ie. velocity) have no basic dependence on grain size(3,19). Although no explanation was given for these observations it is possible that the larger pores associated with the larger grained material would have a direct effect on the Young's modulus by effecting the "b" constant in Equation 2. This effect is considered important and will be considered in the results of this project.

It should be noted that a thorough literature search covering the topics discussed in this report produced no previous research that directly linked high temperature creep damage with ultrasonic sound velocity.

## Chapter IV

## EXPERIMENTAL METHODS

## Samples

The ceramic creep samples used in this study were provided by the National Institute of Standards and Technology . The samples were produced by Standard Oil Engineered Materials Company through a KX-01 reaction-bonded process using siliconized silicon carbide. A reaction-bonding process involves the production of a mouldable body from silicon carbide powder, graphite and a plasticizer. This body is then formed into the required shape by pressing, extruding, injection molding, etc.. The plasticizer is then converted to a porous char by pyrolysis before silicon liquid or vapor is infiltrated to react in situ with the graphite to give a reaction-bonded product.

High temperature creep was introduced into "dogbone" type samples through an applied load resulting in a tensile stress of 100 MPa. The creep tests were performed at temperatures of 1300 and 1375 degrees C for times of approximately 0.25 t, 0.50 t, 0.75 t , where t is the predicted rupture time based upon the Monkman-Grant relationship:

$$\epsilon_s^{1.4554} t_r = 2.364 \times 10^{-6} \quad (3)$$

where  $\epsilon_s$  is the steady state creep rate(9,10). The specimens were loaded under the desired test conditions and the steady- state creep rate measured. After the steady state creep rate was measured, the rupture time ( $t_r$ ) was calculated using the Monkman-Grant equation. Eight samples were then subjected to substained loading for various fractions of the calculated rupture time. The results can be found in Table 1.

All creep testing was performed on "dog-bone" type samples. The gage section was removed from each sample and polished. A typical specimen is shown in Figure 5. The center of each specimen was designated as the location where all ultrasonic readings would be taken. If the specimen had fractured at its center, then a location immediately adjacent to the fracture surface was selected. The thickness of each specimen was recorded at the designated locations using a micrometer readable to the nearest .0001 inch. The thickness measurements were recorded, to be used later in velocity and attenuation calculations, Table 2.

Subsequent to all ultrasonic testing the samples were further polished and micrographs made. The micrographs were used for examining the microstructure of the samples and for determining the density of the material. The material density was calculated using

Table 1: Siliconized Silicon Carbide Creep Test Data  
(Provided by NIST)

| SPECIMEN<br>ID # | STRESS<br>(MPA) | TEMP<br>(C) | STEADY STATE CREEP<br>RATE (1/S)X 10 <sup>-8</sup> | FRACTION<br>OF T <sub>R</sub> | FINAL CREEP<br>STRAIN | LENGTH OF<br>TEST (HRS) |
|------------------|-----------------|-------------|--|-------------------------------|-----------------------|-------------------------|
| 1-2              | 100             | 1375        | 2.28   | 0.27                          | 0.244%                | 23.2                    |
| 1-5              | 100             | 1375        | 3.47   | 0.58                          | 0.359%                | 26.5                    |
| 1-8              | 100             | 1375        | 11.2   | 0.50                          | 0.266%                | 4.3                     |
| 1-9              | 100             | 1300        | 0.553  | 0.50                          | 0.704%                | 343.8                   |
| 1-10             | 100             | 1300        | 0.684  | 0.25                          | 0.381%                | 122.4                   |
| 1-11             | 100             | 1300        | 0.908  | 0.73                          | 0.915%                | 241.1                   |
| 1-12             | 100             | 1375        | 3.58   | 0.25                          | 0.172%                | 11.1                    |
| 2-7              | 100             | 1300        | 0.637  | 0.21                          | 0.315%                | 117.9                   |
| 3-0              | 0               | ----        | ----   | ----                          | 0                     | 0                       |

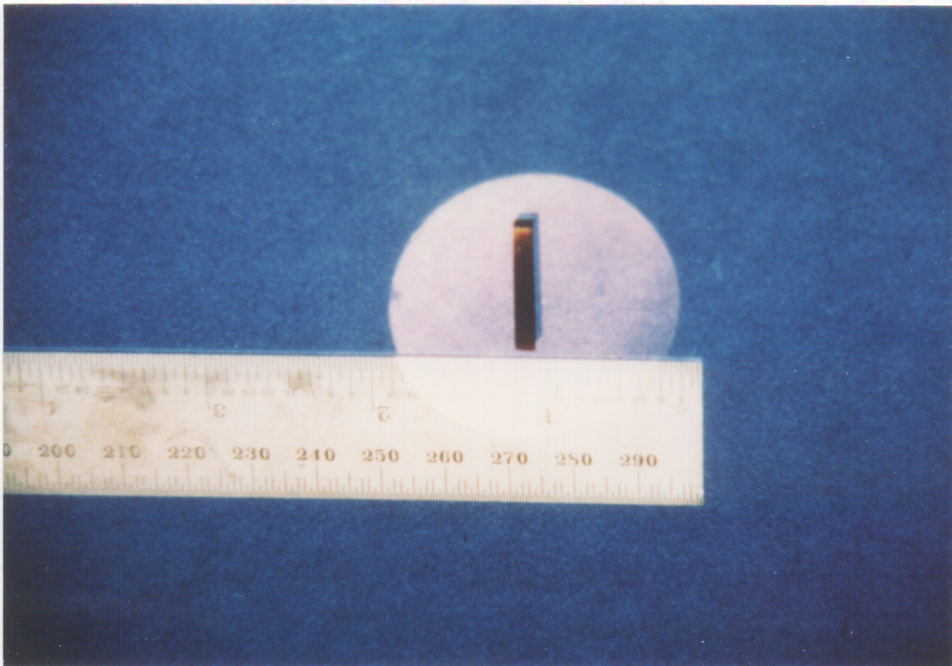


Figure 5:

Gage Section From A Typical Si/SiC Creep Sample

Table 2: Thickness Of Each Sample Measured At The Area to Be Tested Ultrasonically

| SPECIMEN<br>ID # | THICKNESS<br>INCHES |
|------------------|---------------------|
| 1-2              | 0.1154              |
| 1-5              | 0.1170              |
| 1-8              | 0.1161              |
| 1-9              | 0.1169              |
| 1-10             | 0.1187              |
| 1-11             | 0.1141              |
| 1-12             | 0.1172              |
| 2-7              | 0.0972              |
| 3-0              | 0.1198              |



digital image processing equipment. Ten locations on each micrograph were randomly chosen. Cavity density and the volume fraction of cavities was determined for each location and averaged for each micrograph. Cavity density is a measure of the number of cavities, large and small, present per square meter. The volume fraction of cavities is a measurement of the percentage of the entire volume that is cavities. This measurement takes into consideration the size of each cavity where as cavity density does not. Finally the material density was calculated from the volume fraction of cavities measurement. The results of these measurements can be found in the "Results" chapter of this report.

#### Sound Attenuation Measurements

The determination of ultrasonic longitudinal wave attenuation involves the measurement of signal amplitudes and sample thickness. Similar to the velocity measurements performed in this study, a normal incidence longitudinal wave was transmitted into the samples with the resulting back-wall echoes being received. A signal such as that shown in Figure 6 exhibiting an exponentially decaying echo train was necessary for accurate measurements. The amount of attenuation between two signals was calculated as follows:

$$\text{dB Drop} = 20 \log \left( \frac{A_2}{A_3} \right) \quad (4)$$

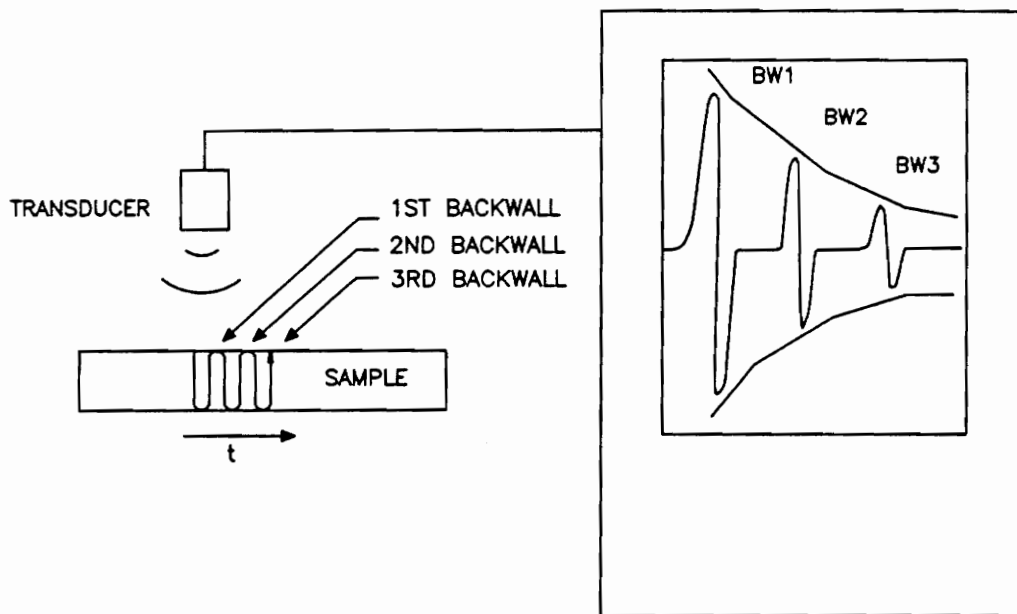


Figure 6:

Exponentially Decaying Echo Train Necessary For  
Accurate Attenuation Measurements

where  $A_2$  and  $A_3$  are the amplitudes of the second and third back-wall reflections. The above equation calculates the relative difference in amplitude between the two signals of interest in decibels. These calculated values must be normalized in order for them to be meaningful due to the varying thicknesses associated with the specimens. This can be accomplished by dividing the relative dB drop experienced by the second signal of interest by the difference in distance traveled by the two signals (ie. twice the thickness of the sample). Thus the following equation was used to define the material attenuation ( $\alpha$ ) constant for each sample:

$$\alpha = \frac{10}{t} \log \left( \frac{A_2}{A_3} \right) \quad (5)$$

where  $t$  is the thickness of the sample at the location of interest (values listed in Table 2). It should be noted that the measurements taken and resulting attenuation values do not discriminate between energy losses due to material effects and other factors such as beam

spread, transducer losses, reflection/refraction losses at sample boundaries, etc. However these secondary losses should remain relatively constant from sample to sample, with any changes in the data caused mostly by material losses only.

A schematic illustrating the experimental setup is shown in Figure 7. The testing apparatus included an immersion tank, Parametric P/R 5600 pulser-receiver, Tektronix 7854 waveform calculator/oscilloscope and Panametrics 75 MHz, .25 inch element transducer. The pulser- receiver transmitted and received electrical signals to and from the transducer. The resulting signals were gated and fed directly into a Tektronix 7854 waveform calculator/oscilloscope where they were digitized, maximum amplitudes measured and attenuation values calculated.

Initial testing of the experimental setup showed that the waveform did not always exhibit decaying back-wall reflections with time. It was determined that because the size of the piezoelectric element in the transducer was much larger than the specimen width, undesirable effects were occurring at the edges of the specimen. This was causing sporadic behavior of the back-wall reflection echo train with small lateral movements of the transducer. It was decided that

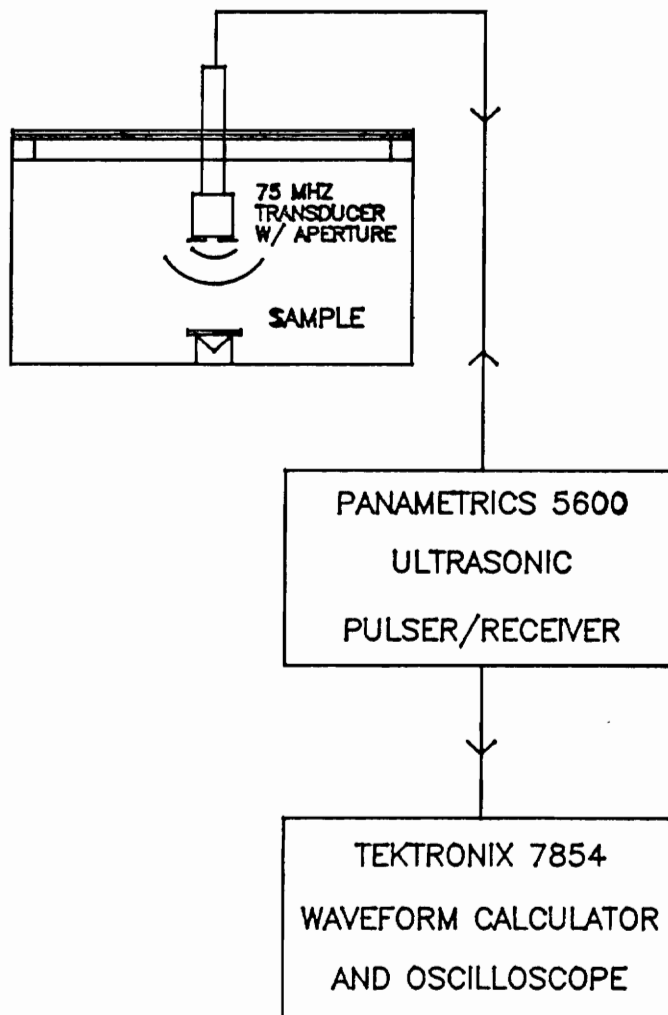


Figure 7:

Schematic Of Equipment Used For Ultrasonic Attenuation Measurements

in order to achieve reproducible measurements the effective size of the ultrasonic beam would have to be reduced to a size significantly smaller than the width of the smallest sample. Another equally important factor was to reduce the near field length to a distance equal to the thinnest specimen. This condition would assure that the reflections being used would originate from at least three times the near field distance as suggested by W.S. Burkl (20). It was decided that an aperture attached to the face of the transducer being used could solve these problems by reducing the beam size of the ultrasound. The aperture consisted of a small hole (.047 inches) drilled through a thin plastic sheet that was attached to the transducer's face as shown in Figure 8. The hole size was calculated so that the near field of the beam was less than the thinnest sample (.0972 inches). The following equations were used for this calculation:

$$N = \frac{.25D^2}{\lambda}$$

(6)

with  $\lambda = \frac{V}{f}$

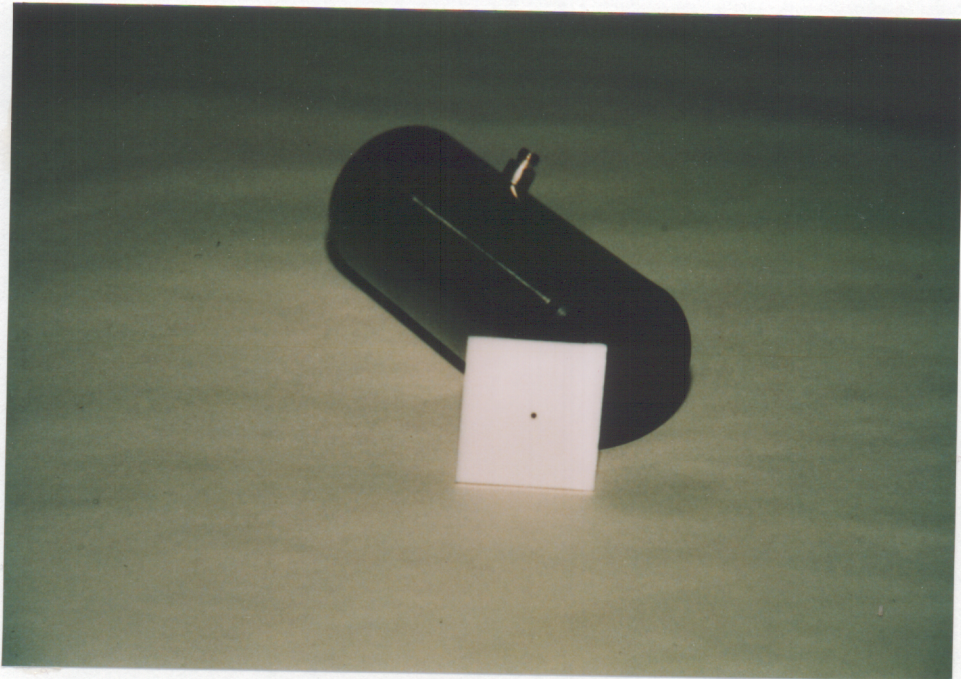


Figure 8:

Transducer/Aperture Used In Attenuation Measurements

where  $N$  is the desired near field distance (.0972 inches),  $V$  is the longitudinal sound velocity in SiC (approx.  $4.3 \times 10^4$  inches/sec.),  $f$  is the center frequency of the transducer (75 MHz),  $\lambda$  is wavelength and  $D$  is the diameter of the element or aperture opening. Sound absorbing foam was used between the aperture and the transducer's face to reduce unwanted reflections off the aperture's surface.

The steps in determining the ultrasonic attenuation values were:

- A sample was placed underwater so that the ultrasonic beam insonified the location where thickness measurements were taken. The transducer was adjusted so that three back-wall reflections were present on the oscilloscope screen. The distance that separated the transducer/aperture's face and the sample was adjusted to a constant .25 inches. The lateral position of the transducer was adjusted so that the ultrasonic beam impinged upon the center (width) of the sample. This was important so that edge effects would not influence the signal. All pulser/receiver adjustments were made to achieve maximum signal amplitude response.



- Once the desired signals were on the oscilloscope screen, they were digitized. The amplitudes of the second and third echoes were measured using the Tektronix 7854 digital oscilloscope. These two values were recorded and the signal delay adjusted so that the signal was slightly repositioned on the oscilloscope screen. The signal was digitized again and the maximum amplitudes recorded. This was repeated five times. The largest values out of the five recorded for both the second and third echoes were used for the attenuation measurement. This procedure was meant to reduce the possibility of error caused by digitizing.
- The material attenuation was calculated using Equation 5.
- A total of 35 different data points were taken for each of the nine samples. Each sample was removed from the tank seven times and replaced to assure repeatability. The large number of data points per sample were taken so that any error due to the digitizing of the signals could be minimized.

### Sound Velocity Measurements

The determination of the ultrasonic longitudinal wave velocity involved a measurement of time  $t$ , and a distance  $d$ , where the velocity is given by:

$$V=4d/t \quad (7)$$

Here  $t$  represents the time required for an ultrasonic wave to make two round trips through the thickness of the material and  $d$  is the thickness of the specimen at the location of interest (values of  $d$  are found in Table 2).

The time of travel,  $t$ , was measured using a pulse-echo overlap method. Figure 9 illustrates the fundamental concepts behind this technique. An ultrasonic pulser-receiver drives a piezoelectric element in the transducer. The resulting signal received by the pulser-receiver is gated, amplified and sent to a dual trace oscilloscope. An oscillator is used to drive one of the horizontal amplifiers of the dual trace oscilloscope. In order to measure the time required to complete two round trips through the specimen, the first and third back-wall reflections were overlaid. This was done

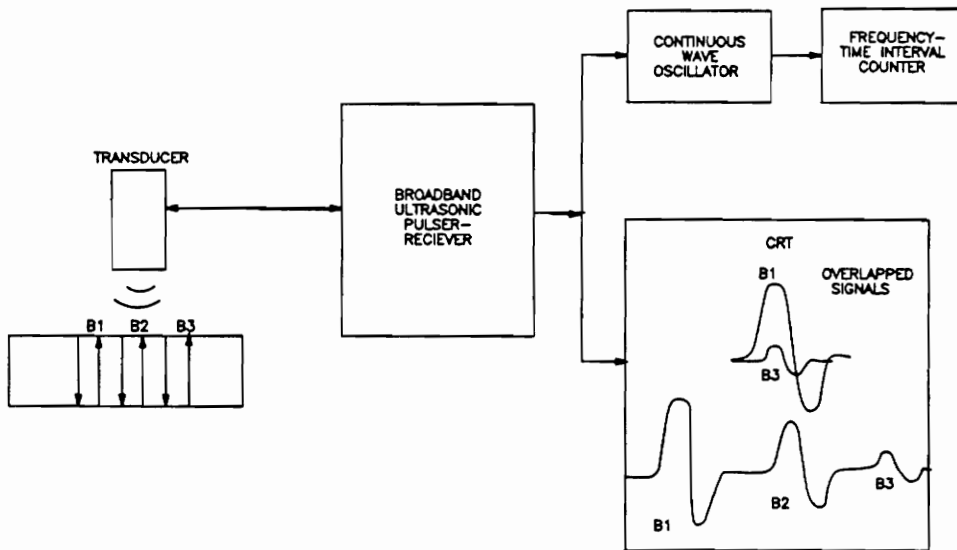


Figure 9:  
Pulse-Echo Overlap Technique

by adjusting the oscillator until the two signals were superimposed on the oscilloscope screen. Overlap occurs when the oscillator frequency is equal to the reciprocal of the time interval between the two reflections. A digital counter is used to read out the time of travel directly. The actual testing setup included an immersion tank, Parametric P/R 5600 pulser-receiver, Parametric 50 MHz transducer with .25 inch element and a Tektronix 2236 oscilloscope as shown in Figure 10. The transducer was positioned so that normal incidence longitudinal waves propagated through the sample. The 2236 oscilloscope was equipped with an internal oscillator and digital counter making the overlap procedures routine.

The steps in determining the material velocity values were:

- A sample was placed in a tank, immersed in water, so that the ultrasonic beam insonified the location that thickness readings were taken. The transducer was adjusted so that multiple back-wall signals were present. The distance that separated the transducer's face and the sample was adjusted so that maximum signal amplitude could be achieved. Initial pulser-receiver adjustments were made in order achieve maximum signal response. These adjustments were not changed until the completion of all velocity measurements.

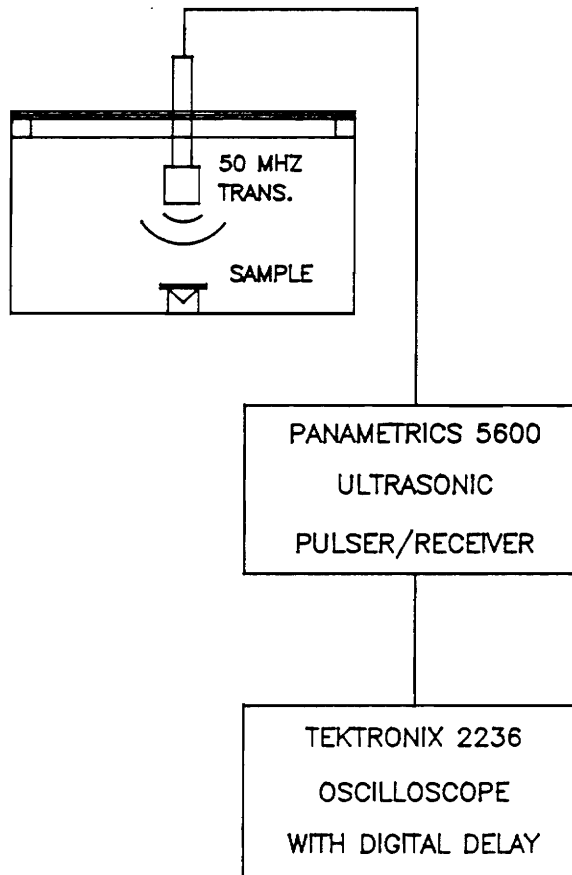


Figure 10:

Equipment Used For Velocity Measurements

- The Tektronix 2236 oscilloscope was equipped with a feature that allowed the operator to digitally measure the time delay between two pulses by electronically overlapping them on the oscilloscope display. To perform this operation the two pulses were overlapped so that their peaks were aligned with one another as shown in Figure 9. Once this condition was met, the actual time separating the two pulses was displayed digitally. The two signals of interest in this investigation were the first and third back-wall echoes that were a result of ultrasound reflecting off the back surface of the sample after traveling through it. Knowing the thickness of the sample at the location of the measurement along with the corresponding time-of-flight measurement, the velocity of the material at that location was calculated.
- A total of 36 different data points were taken for each of the nine samples. Each sample was removed from the tank four times and replaced to assure repeatability. The large number of data points per sample was taken so that any random error due to manual overlapping of the signals could be minimized during analysis.

## Chapter V

## RESULTS

## Microstructural Analysis

Figures 11, 12 and 13 are representative of the micro-structure of the nine creep samples. Figure 11 shows the micro-structure of the original "as received" siliconized silicon carbide. This sample contained no detectable porosity. The micro-structure of the material consisted of silicon carbide grains (dark gray), measuring approximately .005mm wide, surrounded by a pure silicon matrix (light grey). Although some localized variations in the spacing of the SiC grains existed, these were infrequent and widely scattered.

The microstructure of the crept samples, Figures 12 & 13, did not exhibit any increase in SiC grain size. This result was expected since failure of the bonding between grains and deformation of the silicon matrix is believed to contribute to total creep strain. Also, there was no detectable difference in the spacing of the SiC grains when compared to the undeformed sample. There was, however, an introduction of porosity into the microstructure as a result of creep. The porosity was significantly larger in the samples with creep

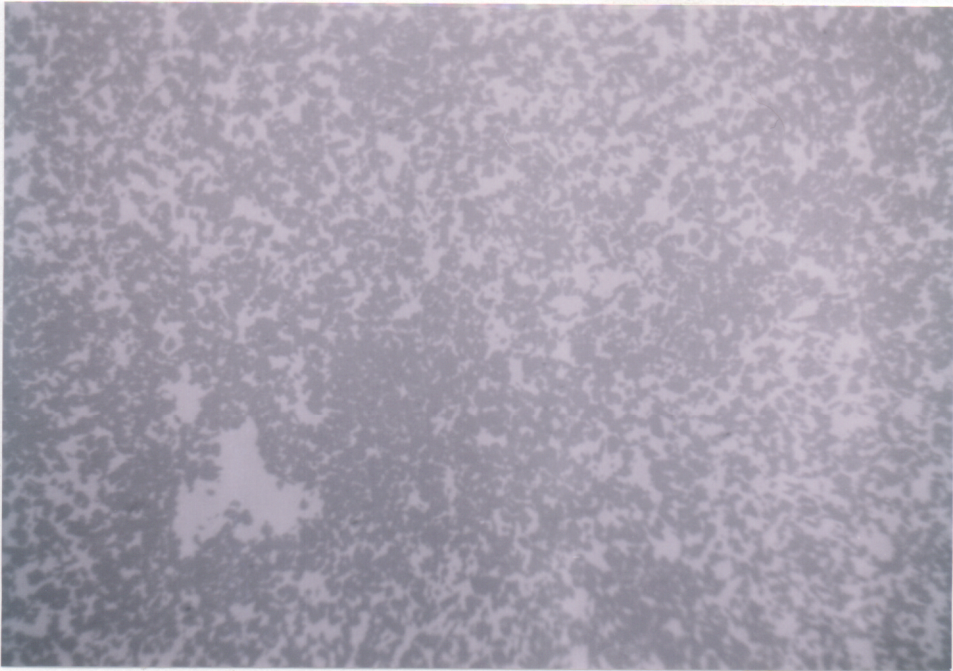
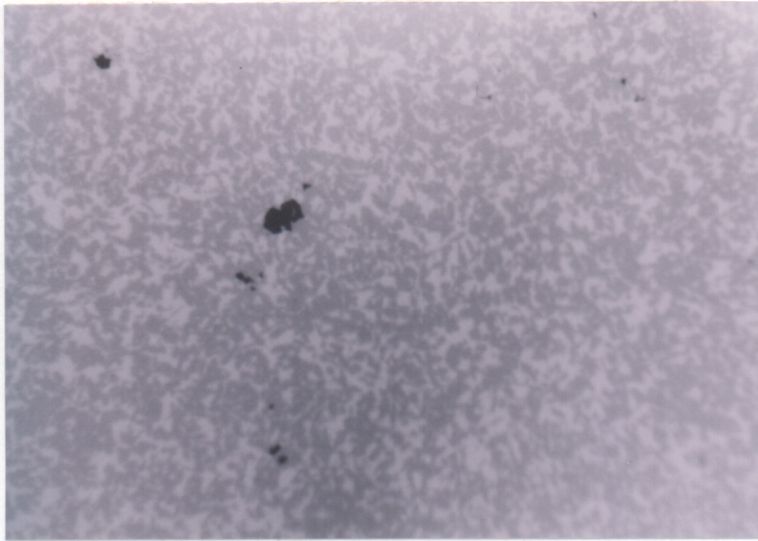


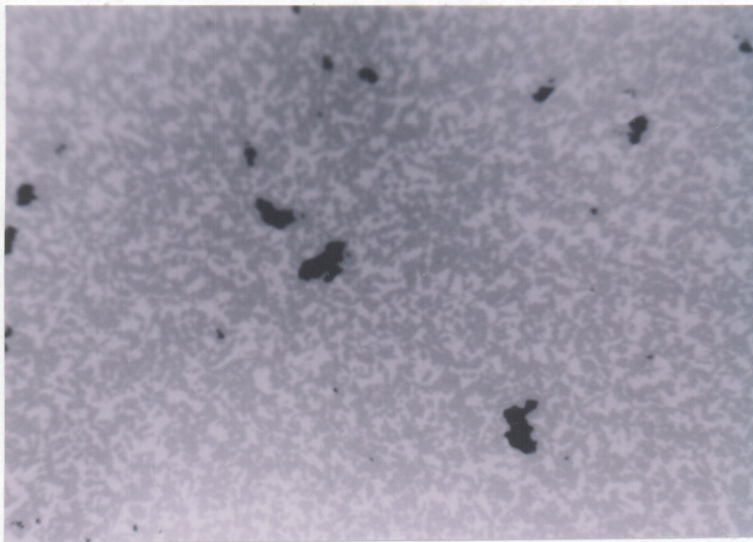
Figure 11:

Microstructure of "As-Received" Siliconized Silicon Carbide  
(200X)





a



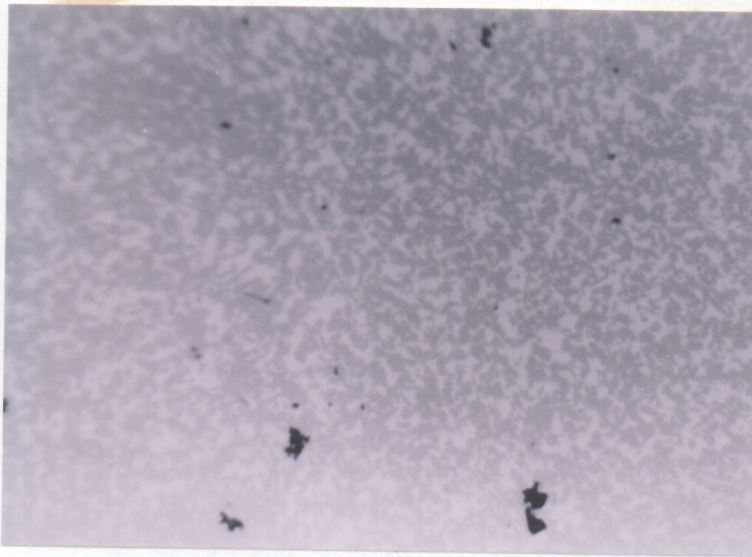
b

Figure 12:

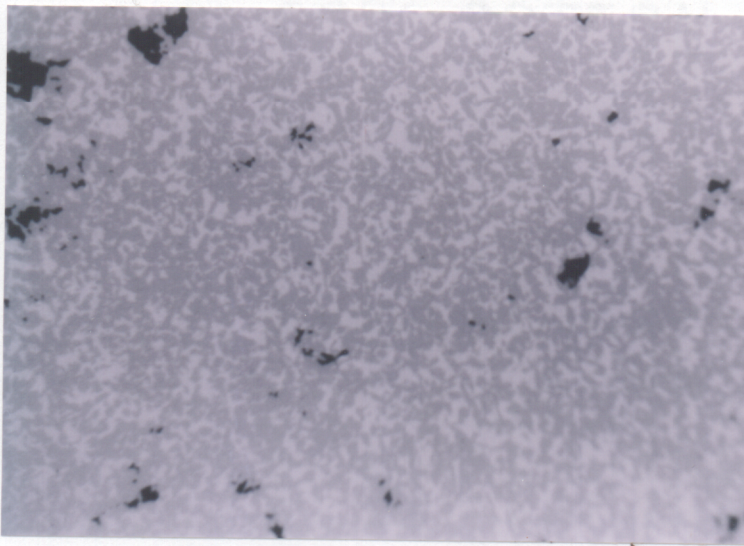
Micrographs of Samples Tested at 1300C (200X);

a) 1-12 Sample (.172% strain), b) 1-2  
Sample (.244% strain)





c

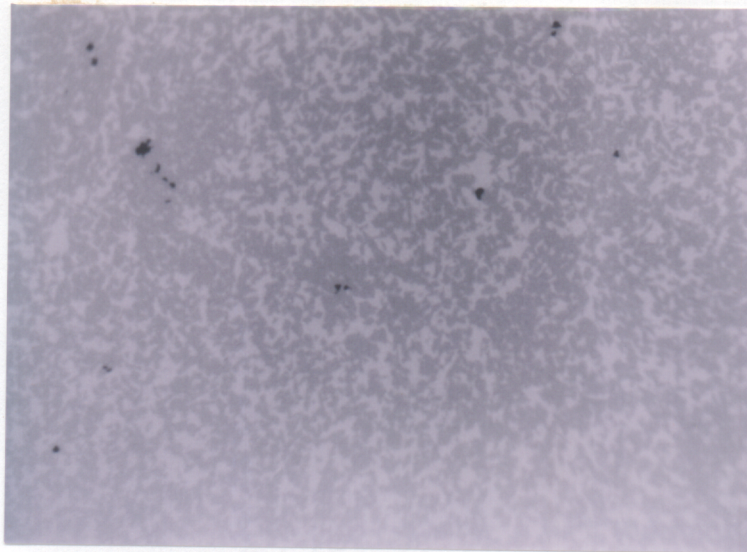


d

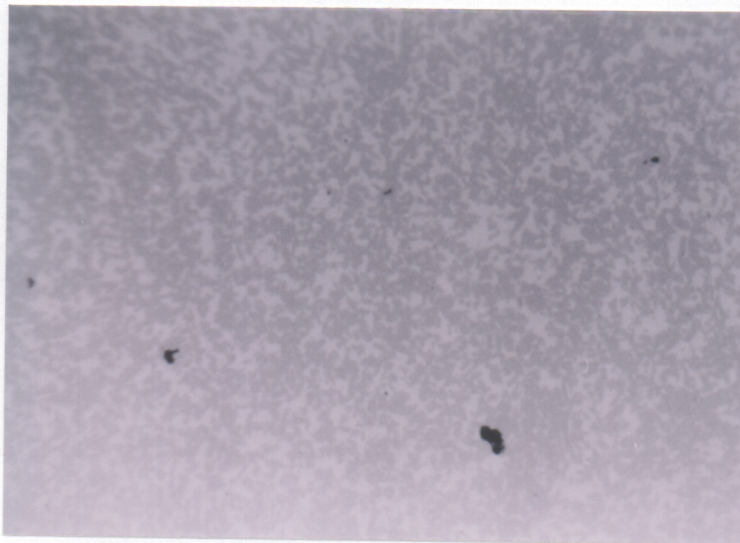
Figure 12 (cont):

Micrographs of Sample Tested at 1300C (200X);  
c) 1-8 Sample (.266% strain), d) 1-5  
Sample (.359% strain)





a



b

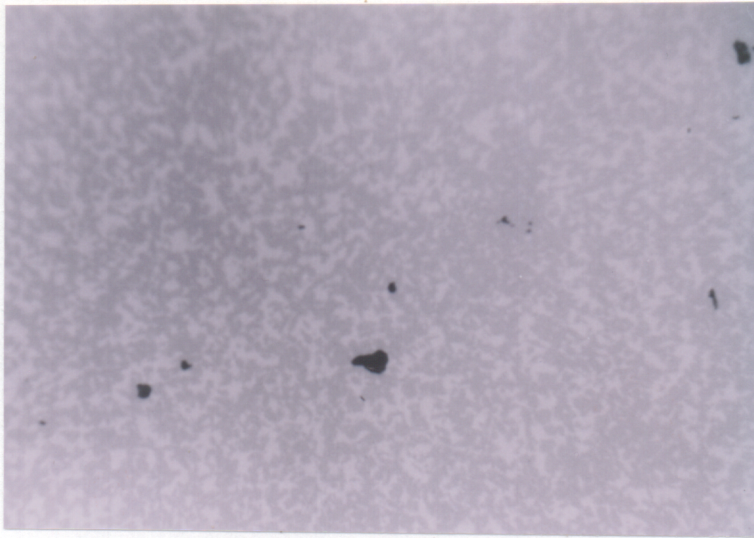
Figure 13:

Micrographs of Samples Tested at 1375°C (200X);

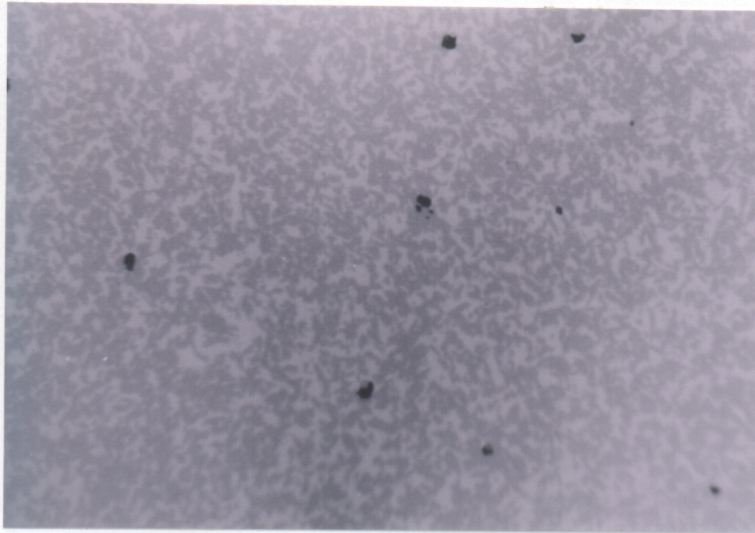
a) 2-7 Sample (.315% Strain)

b) 1-10 Sample (.381% Strain)





c



d

Figure 13 (cont):

Micrographs of Samples Tested at 1375°C (200X);

c) 1-9 Sample (.704% Strain)

d) 1-11 Sample (.915% Strain)

deformation occurring at 1300°C than at 1375°C. This may be due to the inability of the silicon to flow as effectively at the lower temperature, thus resulting in higher negative hydrostatic pressures that formed larger pores. The pores associated with the 1300°C samples ranged from very small up to approximately .03 mm. In contrast, the pores associated with the 1375°C samples ranged from very small up to approximately .01 mm. The pore sizes seemed to increase, at least initially, with creep strain when comparing samples within each temperature set. The pore sizes did not correlate with creep strain if both sets of samples were considered together.

Quantitative measurements concerning the distribution (cavity density) and volume fraction of pores were performed via digital image processing methods. These results are listed in Table 3. Also listed are material density values that were calculated from the volume fraction measurement values (assuming a density for silicon carbide of 2.950 g/cc). Figures 14 and 15 (data provided by S.M. Wiederhorn) are plots of cavity density and volume fraction cavities plotted against the percent creep strain. These plots indicate, first, the cavity

Table 3: Cavity Density, Volume Fraction And Material Density  
Data For Si/Sic Creep Samples

| SPECIMEN | % VOLUME<br>FRACTION<br>CAVITIES | CAVITY<br>DENSITY<br>( $\times 10^9/\text{m}^2$ ) | ESTIMATED<br>DENSITY<br>(g/cc) |
|----------|----------------------------------|---|--------------------------------|
| 2-7      | 0.126                            | 0.15  | 2.946                          |
| 1-10     | 0.267                            | 0.109   | 2.942                          |
| 1-9      | 0.399                            | 0.226   | 2.938                          |
| 1-11     | 0.325                            | 0.290   | 2.940                          |
| 1-12     | 0.166                            | 0.143   | 2.945                          |
| 1-2      | 0.236                            | 0.203   | 2.943                          |
| 1-8      | 0.176                            | 0.195   | 2.945                          |
| 1-5      | 0.356                            | 0.339   | 2.939                          |
| 3-0      | approx. 0                        | approx. 0   | 2.950                          |

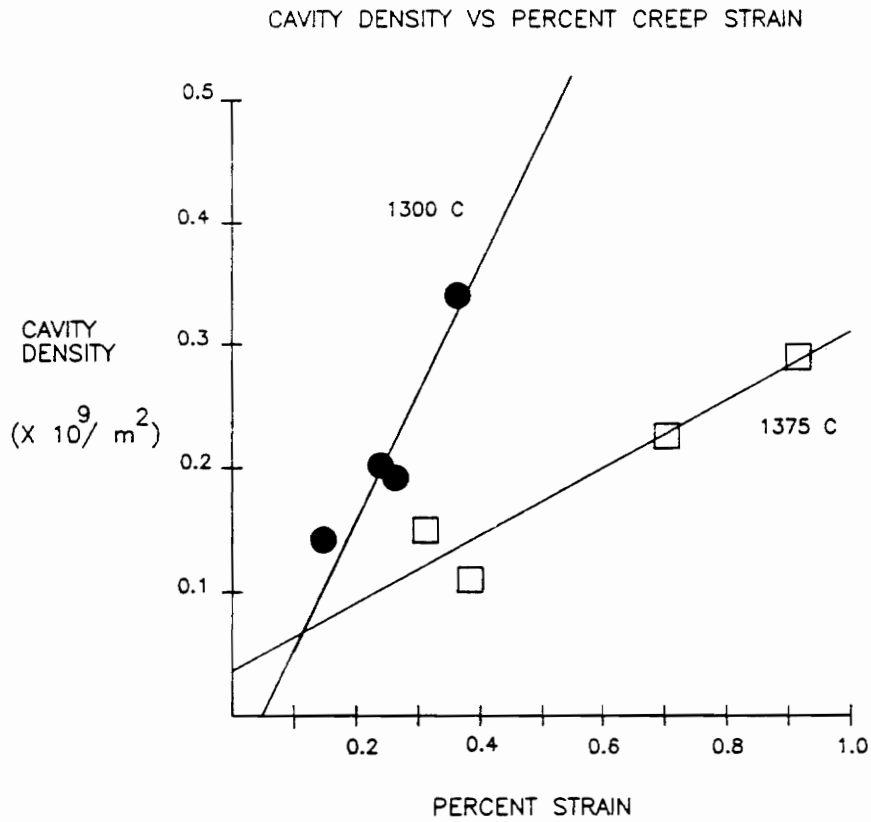


Figure 14:

Cavity Density Verses Percent Creep Strain Plot For All  
Samples Tested

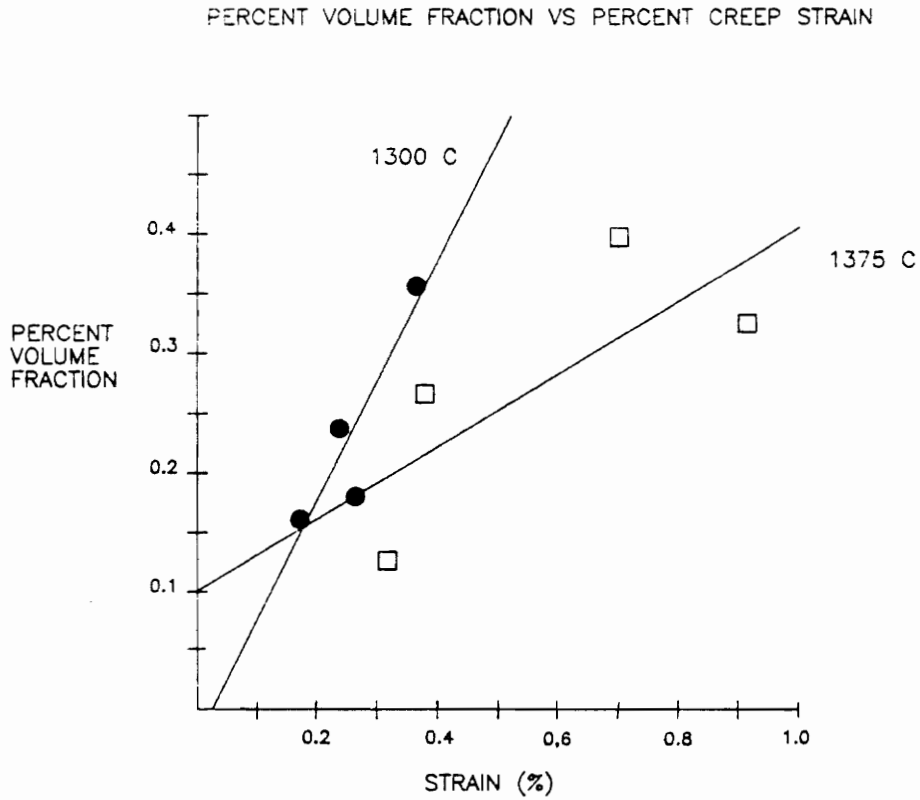


Figure 15:

Volume Fraction Cavities Verses Percent  
Creep Strain For All Samples Tested



density and volume fraction of cavities increase with an increase in strain. Secondly, both of these relationships are temperature dependent. It is clear from these plots that the samples tested at 1300°C contain cavities that not only are more densely distributed but also fill a higher percentage of the total volume than do those contained in the 1375°C samples.

#### Sound Attenuation Measurements

Table 4 shows the average of the ultrasonic data taken on each sample.

The sound attenuation measurements taken on the silicon carbide samples indicated a direct relationship between material sound attenuation and high temperature creep strain. Figure 16 is a plot of material sound attenuation versus percent strain. This plot illustrates that sound attenuation increases with creep strain. An one percent change in creep strain yields a change of approximately 25 percent in sound attenuation. This estimate is determined by considering all samples together regardless of testing temperature. This plot does not indicate that the relationship between sound attenuation and creep strain is dependent upon the testing temperature. An interpretation of this data suggests that the amount

Table 4: Average Ultrasonic Attenuation Data Taken On Each Sample

| SPECIMEN<br>ID# | AVE. ATTEN.<br>(db/inch) | STANDARD<br>DEVIATION |
|-----------------|--------------------------|-----------------------|
| 1-2             | 28.07                    | 3.17                  |
| 1-5             | 28.00                    | 3.06                  |
| 1-8             | 26.78                    | 1.78                  |
| 1-9             | 32.54                    | 2.11                  |
| 1-10            | 27.60                    | 2.24                  |
| 1-11            | 32.99                    | 1.152                 |
| 1-12            | 28.79                    | 2.13                  |
| 2-7             | 29.50                    | 1.89                  |
| 3-0             | 27.73                    | 2.92                  |

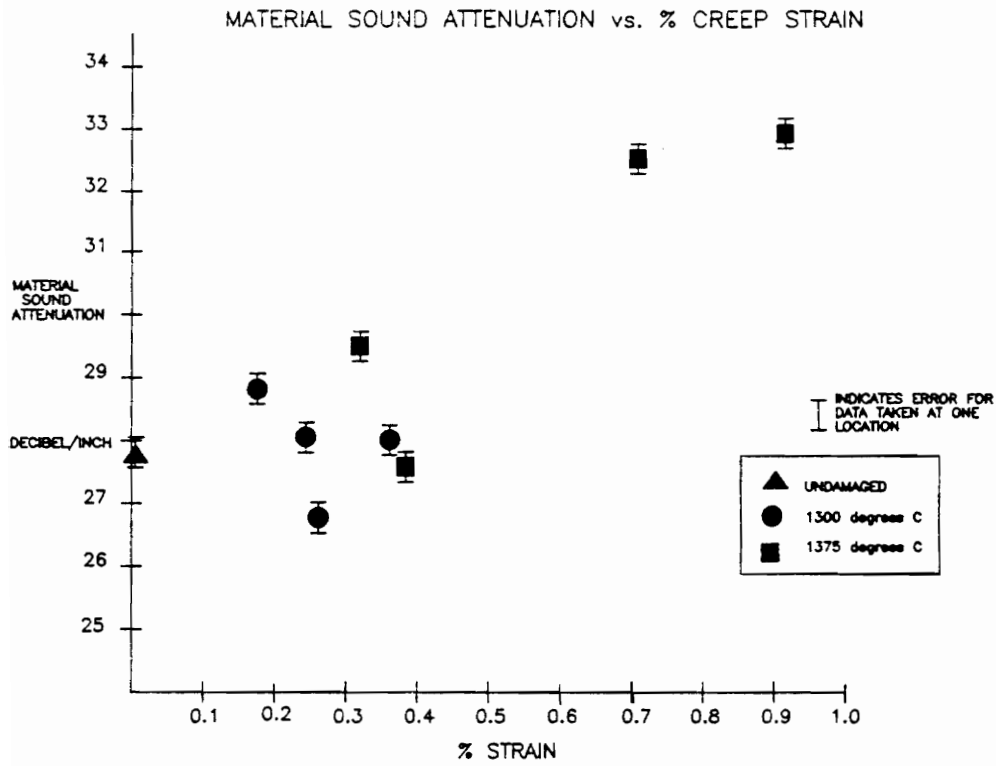


Figure 16:

Material Sound Attenuation Verses Percent Creep Strain

of damage associated with high temperature creep strain can be quantified by ultrasonic attenuation measurements. The following discussion further investigates this relationship.

Figure 17 is a plot of sound attenuation verses cavity density. When plotted against the number of cavities per unit area, the sound attenuation appears to be temperature dependent. In fact, little increase in sound attenuation is observed for the samples tested at 1300°C as opposed to a significant increase for the 1375°C samples. The exact cause of these results is not obvious especially when compared to the microstructural differences of the two sample sets. As previously discussed, the 1300°C samples contained porosity much larger than the 1375°C. This larger porosity also was found to have a more dense distribution. The associated wavelength in this ceramic material using a 75 MHz transducer was approximately .006 inches. Considering this along with the grain and porosity sizes associated with the two sample sets, Rayleigh scattering would be expected. This however, cannot be the case since the samples with the larger, more dense porosity should have greater sound attenuation as a result of Rayleigh scattering.

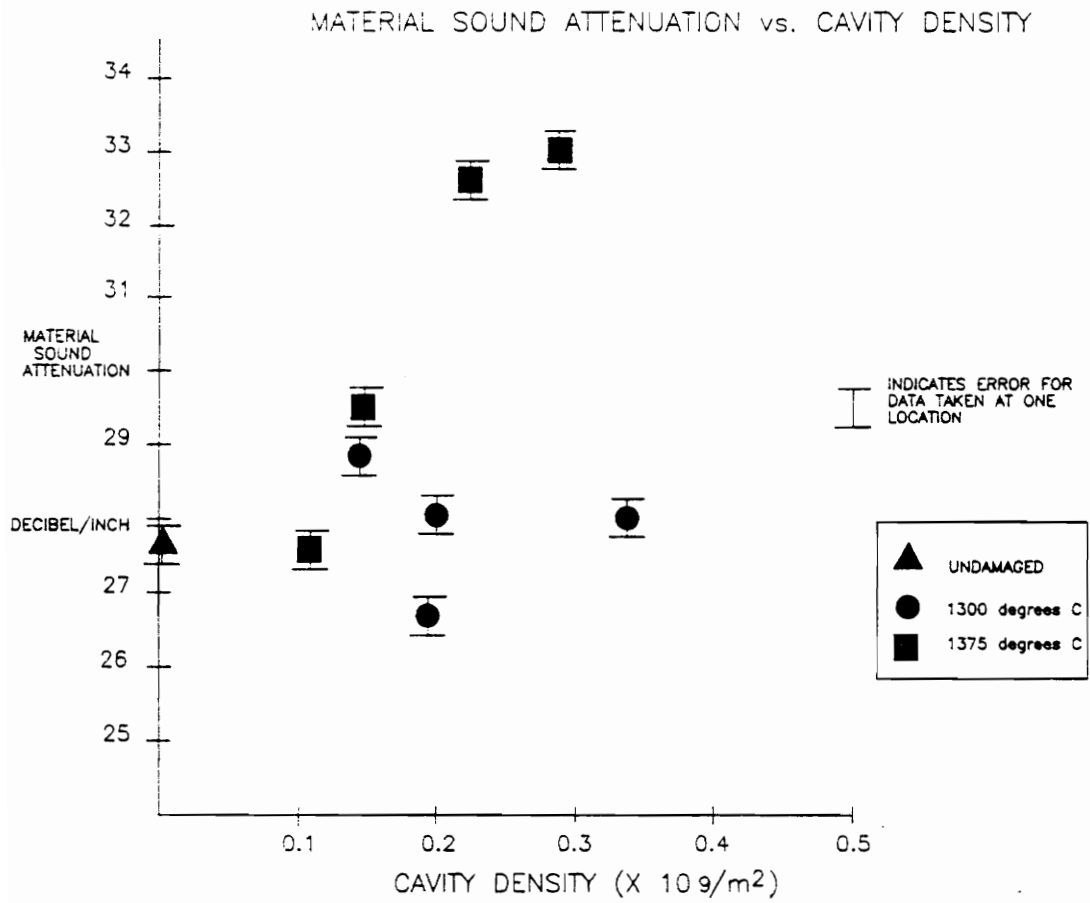


Figure 17:

Material Sound Attenuation Verses Cavity Density

Figure 14 and 15, both show that the range of values measured for cavity density and for the volume fraction of cavities is approximately the same for the two temperature sets. Therefore, another mechanism other than cavity formation must be responsible for the relatively large difference in attenuation measurements between sample sets. Figure 16 indicates that this mechanism is directly related to the amount of creep strain produced in the material. In order to explain this attenuation verse strain relationship, the material must be thought of as a two phase material rather than being homogeneous. The two phases being a silicon carbide structure infiltrated by a pure silicon matrix. It is proposed that the majority of detected high frequency ultrasound is supported mostly by the silicon carbide micro-structure. Propagation through the silicon matrix alone is highly unlikely since the matrix is not always interconnected. The third possible route is for the ultrasound to travel through both the silicon carbide grains and silicon matrix sequentially. This route however would be highly attenuative due to the energy lost at each silicon carbide/silicon interface. Therefore efficient propagation of ultrasound is related directly to the

integrity of the silicon carbide intergranular bonds. As discussed in Chapter 2, creep strain in siliconized silicon carbide involves the two basic processes, failure of silicon carbide intergranular bonding and silicon flow. Therefore, as the strain increases, the bonds between adjacent silicon carbide grains begin to fail. These failures impede the propagation of ultrasound, thereby producing higher attenuation values that are directly related to strain. The porosity found in the samples does not significantly effect the sound attenuation because it always forms in the silicon matrix, thus not adding any additional resistance. Therefore as the strain increases so does the damage to the silicon carbide intergranular bonds which results in an increase in the apparent sound attenuation. It should be noted that these results may change significantly if the frequency of propagated ultrasound is significantly lowered. This would effectively increase the wavelength of the ultrasound possibly making the material behave as though it was homogeneous.

Therefore, it is proposed based upon these results that high temperature creep strain can be determined, independent of the testing temperature, directly from attenuation measurements.

### Sound Ultrasonic Velocity

Table 5 shows the average of the ultrasonic data taken for each sample.

The velocity data taken on the Si/SiC samples exhibited a definite relationship when plotted against percent creep strain. As shown in Figure 18, sound velocity decreases with an increase in percent creep strain. A one percent increase in creep strain produced an approximate 1/2 percent decrease in material velocity. This plot suggests that sound velocity can be used to determine the amount of creep damage present in a material independent of testing temperature. Two approaches will be taken in the following analysis of this relationship. An attempt will be made in determining whether sound velocity is reacting as though the material was homogeneous or a two phase material.

Figure 19 is a plot of sound velocity verses volume fraction cavities. Since microstructural data has shown volume fraction of cavities to be temperature dependent when plotted against strain, this plot should indicate a temperature dependency of velocity as well. This result is suggested by this plot, however due to the narrow range and scatter of the data it was not possible to draw these conclusions definitively.



Table 5: Average Ultrasonic Velocity Data Taken on Each Sample

| SPECIMEN<br>ID# | AVE. VEL.<br>(X $10^5$ in/sec) | STANDARD<br>DEVIATION |
|-----------------|--------------------------------|-----------------------|
| 1-2             | 4.309                          | 0.009                 |
| 1-5             | 4.296                          | 0.008                 |
| 1-8             | 4.302                          | 0.007                 |
| 1-9             | 4.301                          | 0.008                 |
| 1-10            | 4.299                          | 0.010                 |
| 1-11            | 4.297                          | 0.009                 |
| 1-12            | 4.307                          | 0.012                 |
| 2-7             | 4.302                          | 0.013                 |
| 3-0             | 4.314                          | 0.009                 |

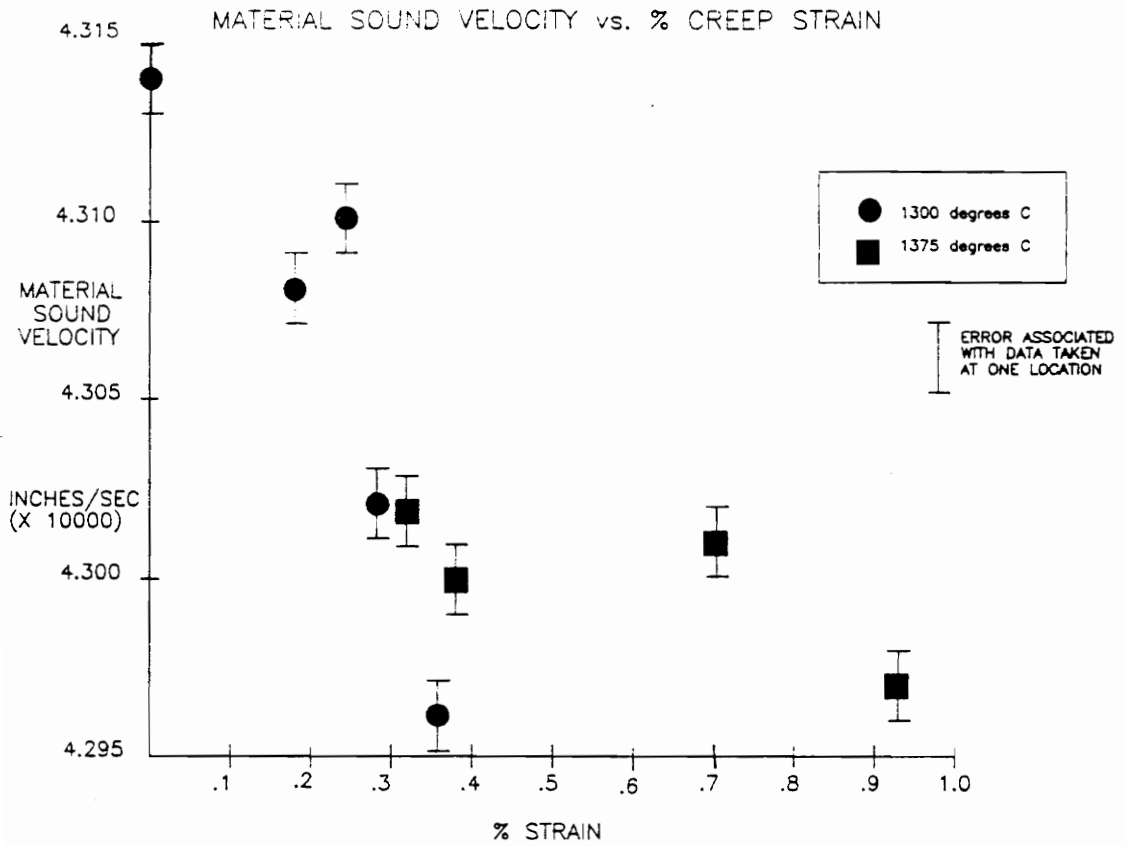


Figure 18:

Material Sound Velocity Verses Percent Creep Strain

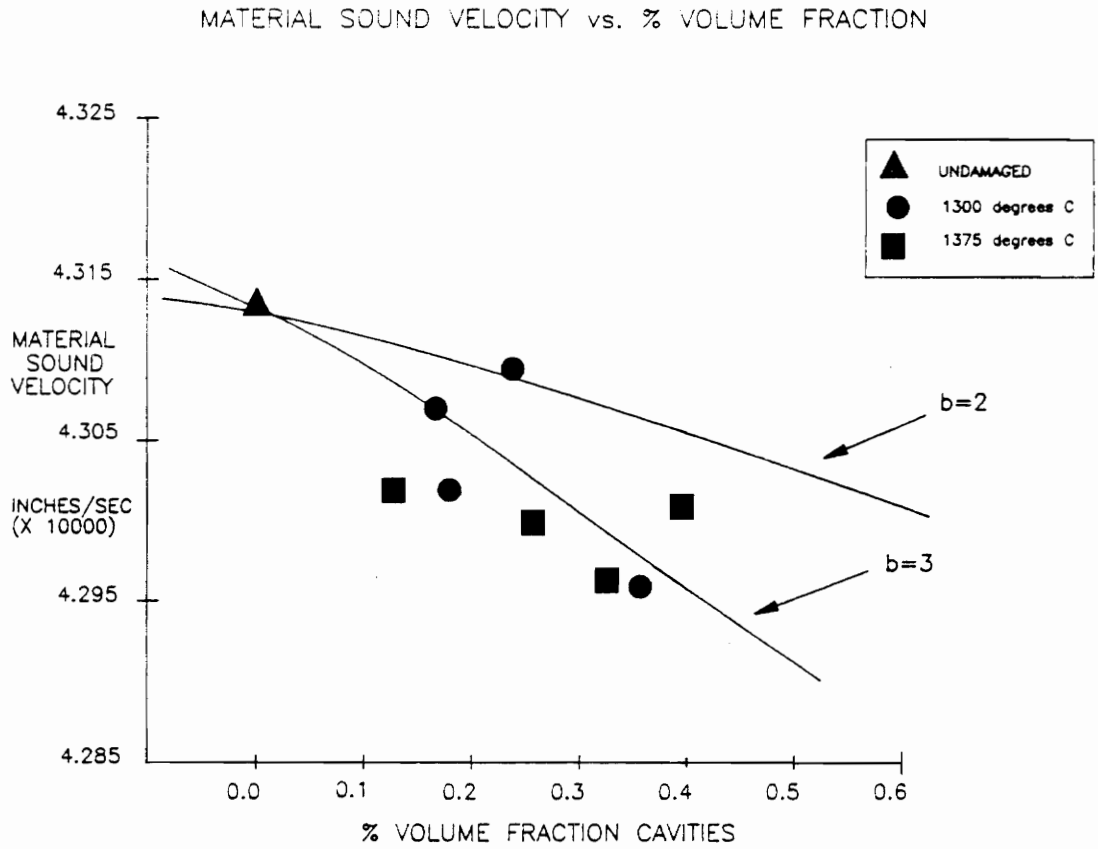


Figure 19:

Material Sound Velocity Verses Volume Fraction Cavities

Therefore it will be stated for discussion purposes, that this plot shows a decrease in sound velocity as the percent volume of cavities increases. This supports the claim that for homogeneous materials, the elastic modulus is exponentially related to the volume fraction of cavities, and that this relationship directly affects velocity. Since density can directly be determined from percent volume fraction, it is clear that if density alone was responsible for velocity changes, then the velocity would increase with an increase in percent volume fraction. Using Equations 1 and 2, and assuming Poisson's ratio to remain constant<sup>(3)</sup>, curves were generated for various values of  $b$ . These curves, as shown in Figure 19, were determined by calculating variations in density as well as Young's Modulus directly from percent volume fraction. This plot illustrates how the observed change in velocity with respect to volume fraction can be represented by Equation 1. Therefore it can be concluded from this information that changes in velocity seem to be controlled by a decrease in Young's Modulus caused by a volumetric increase in the amount of porosity. This conclusion implies that the material effects the velocity as though it were homogeneous. This conclusion contradicts the finding based upon the attenuation results, that porosity does not directly

effect high frequency ultrasonic signals in Si/SiC. This contradiction is addressed by considering the material to act as a composite.

If the material is to be considered a two phase composite, Equations 1 and 2 do not directly apply. Results from the attenuation data suggest that the detected ultrasound travels predominantly through the silicon carbide grains and not through the silicon matrix. Therefore since the matrix material does not significantly effect the signal, formation of cavities within this matrix (silicon) phase also should have no effect. Therefore the relationship illustrated by Figure 19, must be a consequence of another more direct effect on velocity. As previously discussed, porosity occurs subsequent to the failure of a silicon carbide/silicon carbide grain boundary bond. This failure allows for relative movement between grains, thus leading to the formation of a cavity. It is important to realize that associated with every cavity is at least one localized failure site of the silicon carbide interstructure. This suggests that a relationship exists between cavity density and number of failure sites in the

silicon carbide grains. Since an indirect relationship exists between cavity density and cavity volume fraction, the number of failure sites should also be related to the cavity volume fraction. This proposed relationship between cavity volume fraction and SiC bond failures could explain the trends illustrated in Figure 19 since degradation of the SiC interstructure would effectively lower its Young's Modulus. Also, since strain is related to the amount of degradation of the SiC structure, this theory could be used to explain why material velocity decreases with an increase in strain. It should be noted that a theory relating sound velocity and creep strain based upon the above discussion, would be temperature dependent. Temperature has a direct effect on cavity formation due to the increased flow characteristics of the silicon matrix. For instance, the higher the temperature the better the silicon flow, thus resulting in less cavity formation. Therefore the ratio between the number of pores and actual number of bond failure sites will change with temperature at a given strain. In order to test this theory, a theoretical model based on the above discussion was proposed. Here,  $E_0$  is the value of Young's Modulus prior to the introduction of creep strain,  $\rho$  is the density and  $\epsilon$  is creep strain.

$$V_1^2 = \frac{E_0 \exp(-c\epsilon)}{\rho} \quad (8)$$

Equation 8 assumes velocity to be a function of creep strain and density. Here Young's Modulus is related to the amount of strain produced by the material where  $c$  is a constant related to the testing temperature (i.e., the number of grain bond failures to pore ratio). Figure 20 is a plot of material velocity verses strain showing the fit of Equation 8 with different values of  $c$ . This plot was generated by using the appropriate density and strain values while normalizing on the untested sample. This plot suggests that material velocity is a function of strain in siliconized silicon carbide as proposed by Equation 8. This plot also suggests that the results illustrated in Figure 19 were due to a relationship between porosity and SiC bond failure sites which in turn directly effect Young's Modulus. This data suggests that the material sound velocity in Si/SiC is a function

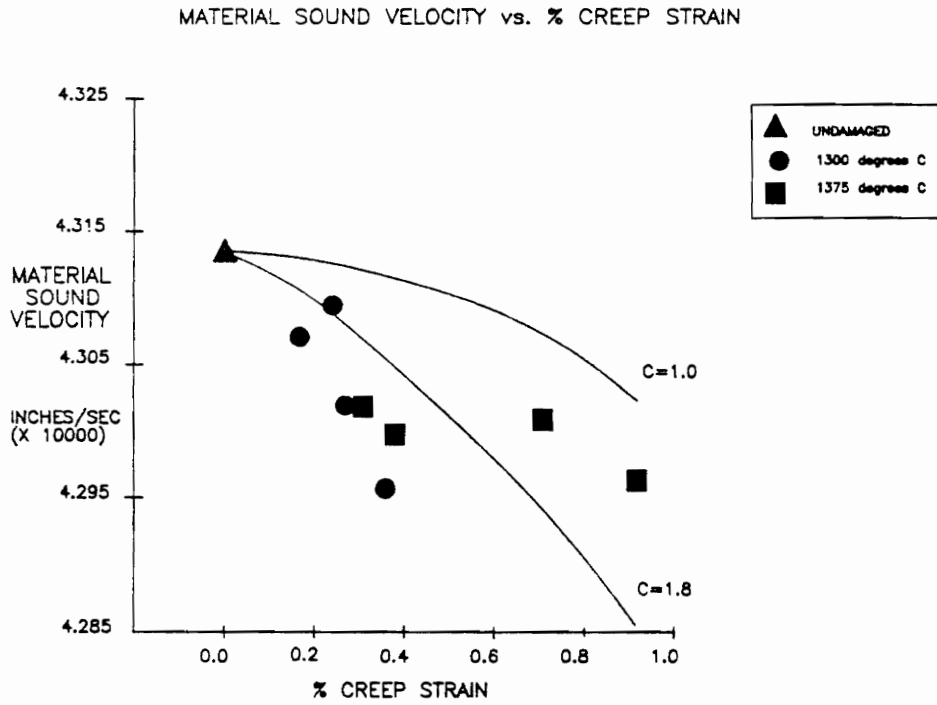


Figure 20:

Plot of Material Sound Velocity Verses Percent Creep Strain Showing Curve of Theoretical Model



of high temperature creep strain and testing temperature where damage directly related to strain effectively lowers Young's Modulus. These results agree with the results obtained with sound attenuation measurements in that they both suggest ultrasound responds to Si/SiC as a composite material.

It should be noted that the model proposed above was based upon a homogeneous model which took into consideration both porosity and density. Since porosity and density are both temperature dependent with strain, the resulting model for Si/SiC was also temperature dependent. However, a conclusion cannot be made, based upon the data, whether or not velocity is temperature dependent with strain.

Finally, material density was calculated from the percent volume fraction cavity measurements and replotted as shown in Figure 21. The result of this plot is of interest because it can directly be compared to previously performed work on single phase sintered silicon carbide. This plot illustrates that as the material density increases so does the sound velocity. This result is similar to those found in studies where sintered silicon carbide samples were purposely manufactured with varying degrees of material density, via porosity.

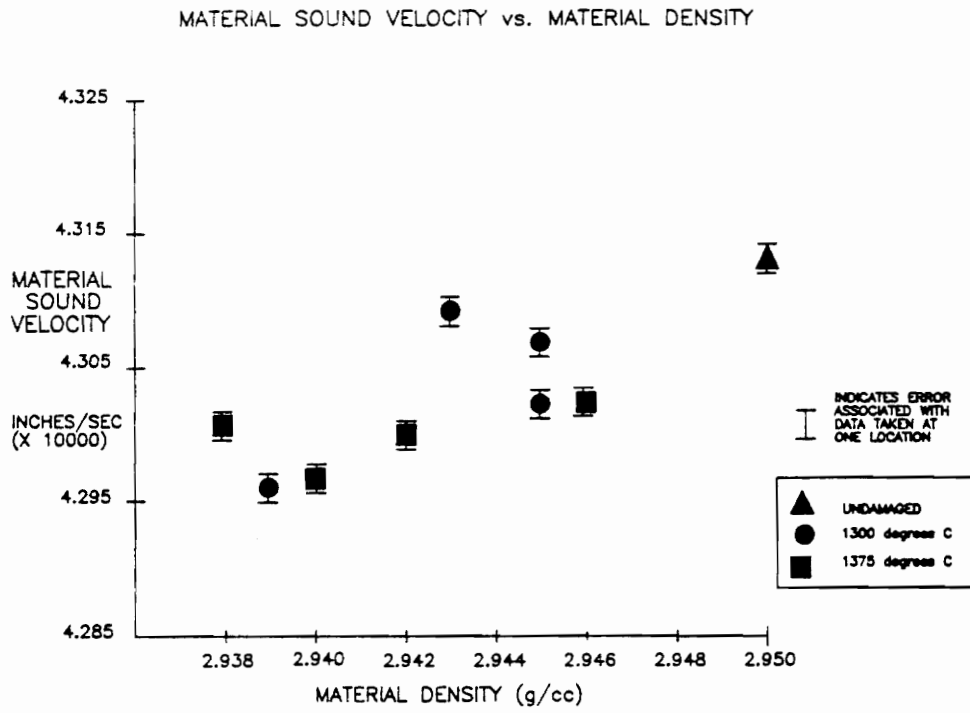


Figure 21:

Material Sound Velocity Verses Material Density

## Chapter VI

## ERROR ANALYSIS

## Ultrasonic Attenuation Measurements

The error associated with all ultrasonic attenuation measurements was estimated to be  $\pm 0.1$  dB/inch. This error is illustrated on various plots throughout this report. This estimate takes into account the accuracy of the instruments and the repeatability of data taken at one location. It should be noted that the material attenuation measured did not account for transmission losses into the water occurring at the back side of the sample and echo to echo (i.e., amplitude dependant). These losses were assumed to remain constant from sample to sample and echo to echo (i.e., amplitude dependent). Therefore this "apparent" attenuation was meant to detect relative change between the samples and was not meant as an absolute measurement. Close attention was given to maintaining a normal angle of incidence between the impinging sound energy and the surface of the sample. Also the distance between the face and the sample surface was adjusted to a minimum and fixed distance so that the attenuation caused by the water couplant would be constant for each sample.

The standard deviations associated with the data scatter are listed in Table 4 and can also be observed on Figure 22. This scatter was a direct result of variations in the measurements taken at different locations on each sample. Examination of this data indicated that the samples tested at 1300 C had an average standard deviation approximately 25% more than the 1375 C samples. The exact cause for this increase is unknown, however it suggests that the degradation of the silicon carbide compact is not as evenly distributed at the lower strains.

#### Velocity Measurements

The error associated with all ultrasonic velocity measurements was estimated to be  $\pm 0.001 \times 10^5$  in/s and is illustrated on various plots throughout this report. This value accounts for error associated with the equipment used as well as for human error. Human error was involved in these measurements due to the subjective nature of the overlap technique used. This was reduced as much as possible by practicing the technique on known samples and comparing results prior to collecting data. Transducer angle and distance from the sample were both controlled as described for the attenuation

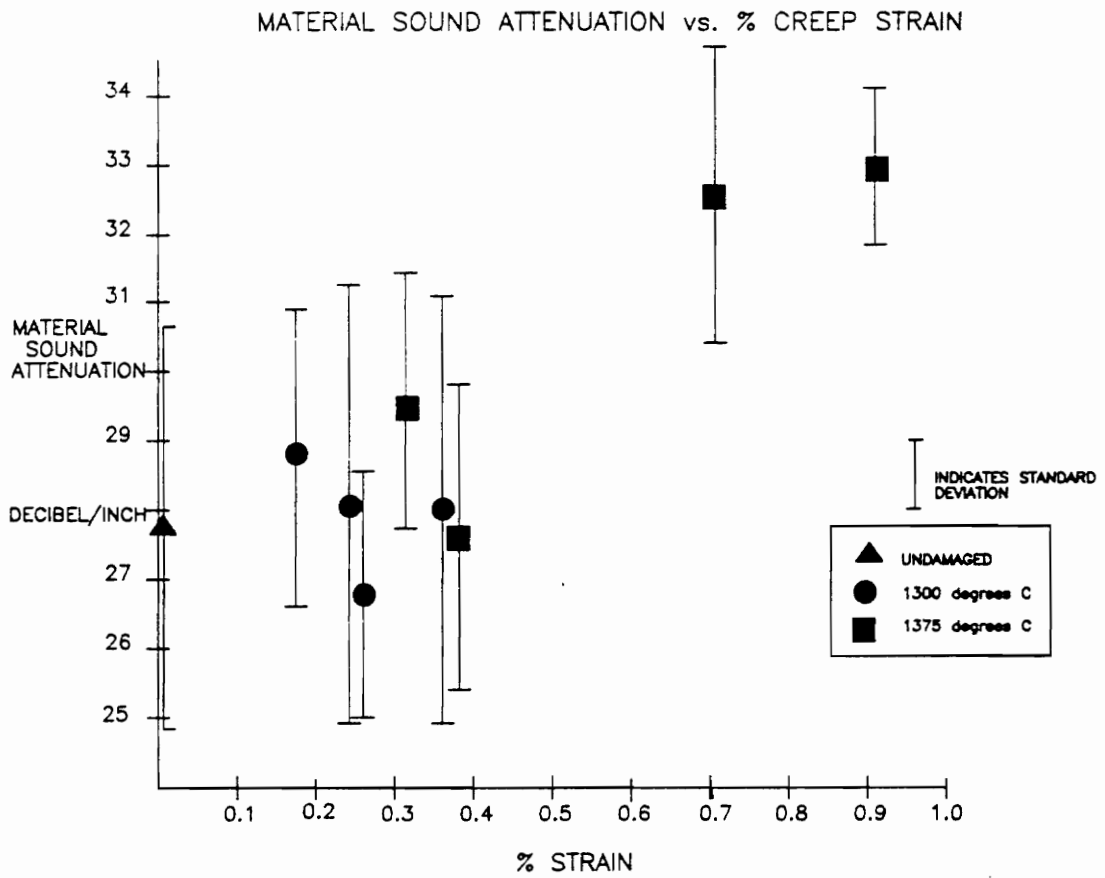


Figure 22:

Plot Illustrating The Scatter In Attenuation Data Associated With Measurements Taken At Different Locations

measurements. However, the velocity measurements did not seem as sensitive to such variations when compared to attenuation measurements. Because the time measurement performed in this study was a difference in arrival time between the front and back surface echoes, water temperature had no effect. The standard deviations associated with the data scatter are listed in Table 5 and can also be observed on Figure 23. No significant difference was observed in the scatter associated with both sample sets.

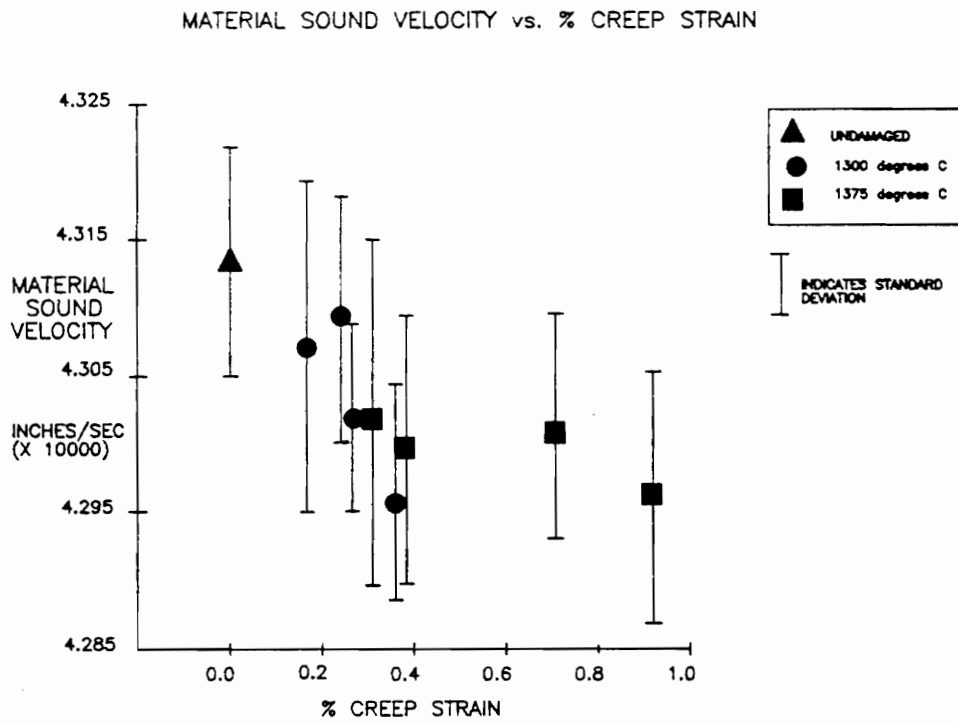


Figure 23:

Plot Illustrating The Scatter In Velocity Data  
Associated With Measurements Taken At Different Locations

## Chapter VII

## CONCLUSIONS

High temperature creep of the Si/SiC samples yielded the formation of porosity in the microstructure of the sample. This porosity formed only in the silicon phase with little damage to the individual silicon carbide grains being observed. The size as well as distribution of the porosity was greater in the samples tested at 1300°C than at 1375°C. An increase in the volume fraction and density of the porosity was observed with an increase in creep strain. These relationships were found to be temperature dependent.

Both velocity and attenuation results suggest that high frequency ultrasound responds to Si/SiC as a two phase material and not as a homogeneous medium. It was concluded that detectable high frequency sound energy travels predominantly through the silicon carbide grains and not through surrounding silicon matrix.

A direct relationship was found between ultrasonic attenuation and creep strain. Sound attenuation increased with an increase in creep strain. This relationship was not effected by the severity of the porosity found in the microstructure. It was proposed that an



increase in attenuation is caused by an increase in SiC/SiC intergranular bond failures with an increase in creep strain. This result suggested that high frequency sound energy propagates primarily through the silicon carbide interstructure and not through the surrounding silicon phase where cavity formation occurs.

Material velocity measurements also indicated a direct relationship with creep strain. This relationship showed material velocity decreasing with an increase in creep strain. A model was developed based upon the theoretical results of a similar model relating porosity in a homogeneous material. This model showed material velocity to be effectively a function of Young's modulus and density. It was proposed that Young's modulus is exponentially related to creep strain through a mechanism of failures in the intergranular bonding of the silicon carbide interstructure. The model suggests that material sound velocity is temperature dependent with creep strain.

It can be concluded from this study that both high frequency sound attenuation and velocity are both related to creep strain and could be used in evaluating the amount of creep damage present in Si/SiC. It should be noted that sound velocity measurements are less sensitive to various testing variables and may produce a more reliable test.

## REFERENCES

1. M. M. Dobson, "Silicon Carbide Alloys," Research Reports in Material Science, Parthenon Press.
2. V. Krishnamachari and M.R. Notis, Interpretation of High-Temperature Creep of SiC by Deformation Mapping Techniques, Materials Science and Engineering, No 27, 1977.
3. S. J. Klima and G. Y. Baaklini, "Nondestructive Characterization of Structural Ceramics," SAMPE Quarterly, April 1986.
4. B. Wilshire, "Creep of Ceramic Materials," Creep of Engineering Materials, 1978.
5. G. Simon and A.R. Bunsell, "The Creep of Silicon Fibres", Journal of Materials Science Letters, Vol 2, 1983.
6. A. S. Jayatilaka, "Fracture of Engineering Brittle Materials", Applied Science Publishers LTD, 1979.
7. B. Holt, "Selecting Materials for Temperature Resistance," Guide To Engineering Materials, 1987,pg. 58.
8. Tze-Jer Chuang and Sheldon M. Wiederhorn, "Damage-Enhanced Creep in a Siliconized Silicon Carbide: Mechanics of Deformation", Journal of American Ceramic Society, Vol. 71, 1988, 595-601.
9. S. M. Wiederhorn, L. Chuck, E.R. Fuller Jr., and N.J. Tighe, "Creep Rupture of Siliconized Silicon Carbide", Tailoring Multiphase and Composite Ceramics, Plenum Pub., 1986.
10. S. M. Wiederhorn, D.E. Roberts, and Tze-Jer Chuang, "Damage-Enhanced Creep in a Siliconized Silicon Carbide: Phenomenology", Journal American Ceramic Soc., Vol 71 1988, 602-608.

11. B. J. Hockey and S. M. Wiederhorn, "Effect of Microstructure on the Creep of Reaction Bonded Silicon Carbide", Submitted to American Ceramic Society, Sept 11, 1989.
12. S. Serabian and R. S. Williams, "Experimental Determination of Ultrasonic Attenuation Characteristics Using the Roney Generalized Theory," Materials Evaluation, July 1978.
13. E. P. Papadakis, "Ultrasonic Attenuation Caused by Scattering in Polycrystalline Media," Physical Acoustics, Volume IV, 1968.
14. S. J. Klima, "NDE for Heat Engine Ceramics," NASA-TM-86949.
15. G. Y. Baaklini, E. R. Generazio and J. D. Kiser, "High-Frequency Ultrasonic Characterization of Sintered Silicon Carbide," J. Am. Ceramic Soc, Vol.72, 1989.
16. S.J. Klima, G.K. Watson, T.P. Herbell and T.J. Moore, "Ultrasonic Velocity for Estimating Density of Structural Ceramics", NASA-TM-82765.
17. R. W. Rice, "Microstructure Dependence of Mechanical Behavior of Ceramic," Properties and Microstructure, R.K. MacCrone, ed., Academic Press, 1977.
18. G. Y. Baaklini and P. B. Abel, "Radiographic and Ultrasonic Characterization of Sintered Silicon Carbide, Materials Evaluation, October 1988.
19. C. O. Ruud and R. E. Green Jr., "Nondestructive Methods for Material Property Determination," Proceedings of a Symposium on Nondestructive Methods for Material Property Determination held April 6-8 1983, Hershey PA. Plenum Press, NY.
20. W. S. Burkle, "Measurement of Ultrasonic Longitudinal Wave Attenuation," Materials Evaluation, Vol. 42, 1984.

## VITA

Jonathan D. Buttram was born on October 3, 1962 in Roanoke Virginia. He entered Virginia Polytechnic Institute and State University in September 1981 and received his Bachelor's degree in Engineering Science and Mechanics in 1985. Immediately following the completion of his Bachelor's degree, he entered graduate school where he worked towards a Master's degree until January 1987. Between January 1987 and September 1989 he worked at Babcock and Wilcox's Lynchburg Research Center as a Research Engineer. During this time he worked on his Master's Thesis which he is using towards the completion of his Master's of Science degree in April 1990. He has authored one technical paper and coauthored two patent disclosures.